THE NUCLEAR DECAY SCHEMES
OF
GOLD-198 AND GOLD-199

A Thesis

Submitted to

the Faculty of Graduate Studies

In Partial Fulfillment

of the Requirements for the Degree

Master of Science

at

The University of Manitoba

by

Werden J. Keeler

February 1964

ACKNOWLEDGEMENTS

The author wishes to extend his sincere thanks to Dr. R. D. Connor for his helpful and enthusiastic supervision throughout this work. Thanks are also due to Mr. W. Van Wyngaarden and and Mr. C. R. Cothern for their constructive discussions, and to Mr. R. Verrall for his generous assistance with the computer programming.

I would like to express my gratitude to the University of Manitoba Physics Department, and to the National Research Council for financially supporting me in this work, to Mr. F. Konopasek for his assistance with the electronics, and to Miss M. Shabbits for typing the manuscript.

ABSTRACT

Recently, interest has been revived in two aspects of the Au^{198} decay scheme. These are: (a) the shape of the dominant β-transition from the ground state of Au^{198} to the first excited state in Hg^{198}, and (b) the experimental values of the internal conversion coefficients of the 412 kev. transition in Hg^{198}, which is known to be pure E2.

The radioactive isotopes Au^{198} and Au^{199} are investigated, with primary consideration being given to the Au^{198} isotope. The Au^{199}, which appears as a contaminant in Au^{198}, is investigated as a precursor to the main work, in order to establish proper contaminant subtraction from the Au^{198} spectrum. The experimentally determined properties of the Au^{199} isotope are discussed in the Appendix and are compared with the results of other workers.

The first part of the thesis discusses some theoretical aspects of beta decay, the instrumentation used in the beta investigations, and the source preparation technique developed for precise beta investigations. The second part of the thesis is devoted

to analysis of the Au^{198} data, and interpretation of the results.

The Au^{198} continuum is found to exhibit the allowed shape. At the same time, using the Peak to Beta Spectrum technique, the conversion coefficients for the 412 kev. transition in Hg^{198} are found to be in complete agreement with theory. The results are tabulated and compared with those of other investigators. A possible explanation is given for the disagreement between the predicted conversion coefficients and those obtained experimentally by other workers who have used the P.B.S. technique.

TABLE OF CONTENTS

Chapter V

Present Investigations

Chapter VI

Shape Factors for the Au^{198} 960 kev. β-Feed

Appendix

Chapter I

THEORETICAL CONSIDERATIONS

Introduction:

The existence of beta (β) and gamma (γ) radiation emitted in the decay of radioactive elements, became known very soon after the discovery of radioactivity by Becquerel in 1896. The energy spectrum of the β-radiation was found to contain both a continuous component and discrete lines. The former was completely unexplainable at first, whereas the line spectra were found in 1920 to be due to atomic electrons interacting with the excited nucleus. Because the β-line "series" occurred at energies corresponding to the difference in energy between the atomic shells, it was concluded that the β-lines were photo electrons expelled by monochromatic γ quanta emitted from the nucleus. Later when conversion electron theory was developed, this simple explanation was abandoned. Instead, electron conversion must be considered an additional mode by which excited nuclei decay. Thus the excited state of a nucleus can de-excite by emission of γ quanta or by direct interaction with the atomic electrons.

In 1934 the first acceptable theory for the continuous spectrum was presented by Fermi. It was based on the neutrino hypothesis first suggested by Pauli, and paralleled Fermi's earlier work on photon emission. The theory preserved the laws of Conservation of Energy and Momentum which were put in jeopardy by the interpretation of existing data at that time. The experimental facts indicated that although the parent nucleus was in a definite energy state, as was the daughter nucleus, the energy of the emitted electron was not necessarily equal to the difference between the energy of the nucleus before and after emission, but could have any value between zero and the total disintegration energy between the two states.

It seemed that momentum was not conserved either, since from cloud chamber and photographic emulsion experiments it was observed that the β-particle was usually emitted at an angle other than 180° to the track of the recoiling nucleus.

With the development of Wave Mechanics, the property of intrinsic angular momentum or spin of the particles became of interest. If the initial nucleus A emits a β-particle leaving a product nucleus B, the angular momentum of the system (B + β) consists of

three parts; the angular momentum of B, its rotational angular momentum with that of β about their common center of mass, and the spin of β. For the total angular momentum to be conserved, the resultant of these three contributions must be equal to the angular momentum of the initial nucleus A. Since the mass no. of B equals that of A, its angular momentum must equal that of A or differ from it by an integral multiple of $h/2\pi$. The second contribution due to rotational angular momentum, can only be zero or an integral multiple of $h/2\pi$ and finally, the spin of the β-particle (electron or positron) is known to be $1/2(h/2\pi)$. When two or more angular momenta are added, the resultant is either equal to the sum of the components or is less than the sum by an integral multiple of $h/2\pi$. However, when the three contributions are added in accordance with this rule, it is found that the total angular momentum of the system (B + β) must differ from that of A by an odd multiple of $1/2(h/2\pi)$.

Therefore, to preserve the laws of Conservation of Energy, Momentum, and Angular Momentum, the neutrino (ν) was postulated as being a third particle in the process of beta decay. Each β-decay event is accomplished by the release of a total amount of energy equal

to the end point energy of the spectrum. This energy is shared between the β-particle, the neutrino, and the recoil nucleus, but the energy of recoil is usually negligibly small relative to that ascribed to the β-particle and neutrino. The neutrino was postulated to have spin 1/2(h/2π), to be electrically neutral in order to conserve charge during β-decay, and to have a vanishingly small rest mass. The neutrino has such a small interaction cross-section with other matter that for 25 years it defied positive identification. Not until the recent (1956) reports of Reines and Cowan[1] can the neutrino be said to have been detected experimentally. Thus, for

β^- emission, $^{n}_{p}A^{q} \longrightarrow {}^{n-1}_{p+1}B^{q} + e^- + \text{neutrino}$ . . (I - 1)

β^+ emission, $^{n}_{p}A^{q} \longrightarrow {}^{n+1}_{p-1}C^{q} + e^+ + \text{neutrino}$ . . (I - 2)

where p is the number of protons in the parent nucleus, n the number of neutrons, q the atomic mass, $e^{\mp}$ the emitted β-particle, and B or C the daughter nucleus.

The neutrino was assigned Fermi-Dirac statistics as well, for without the neutrino the number of particles in the system before and after β-transformation differs by one unit. This implies that the statistics for the system would change either from Fermi-Dirac to Bose-Einstein, or vice-versa. The neutron, proton, and

electron are known to obey Fermi-Dirac statistics so that the existence of the neutrino with Fermi-Dirac statistics, conserves the statistics of the system.

(1) Beta Decay:

Illustrated in fig. 1(a) is a typical β-transition. Fig. 1(b) illustrates the associated momentum continuum. The end point and continuous momemtum distribution both indicate the process is one in which the total available energy is shared by two particles, the β-particle and the neutrino. The upper energy end point corresponds to the case where the β-particle receives all the available energy. It is determined from a Fermi analysis (to be discussed below) and its determination yields a value of the total transition energy for the beta decay process.

In the analysis of the β-continuum it is assumed that;

(1) the β-particle and neutrino are emitted simultaneously,

(2) the particles are relativistic,

(3) the recoil energy of the nucleus is negligibly small.

The momentum distribution can then be represented

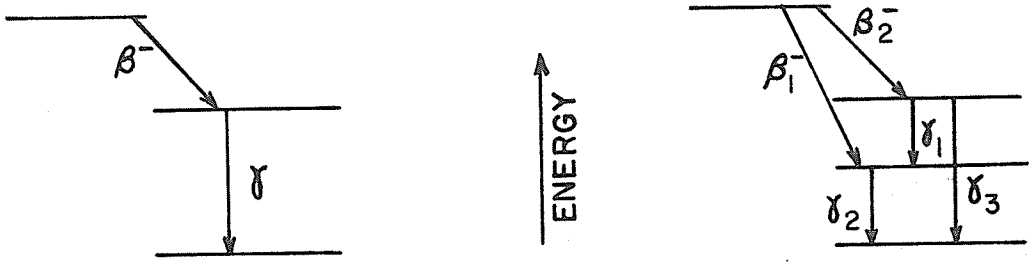

A: SINGLE β FEED

TWO β FEEDS

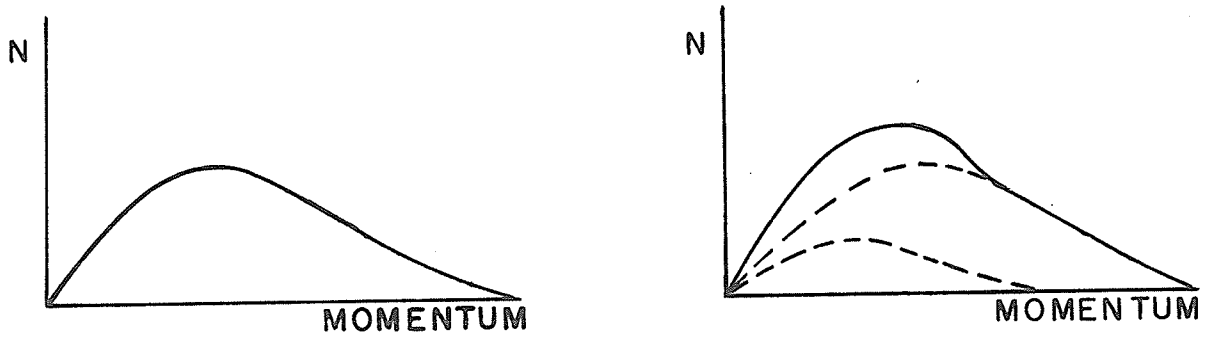

B: NORMALIZED SPECTRUM

NORMALIZED SPECTRUM

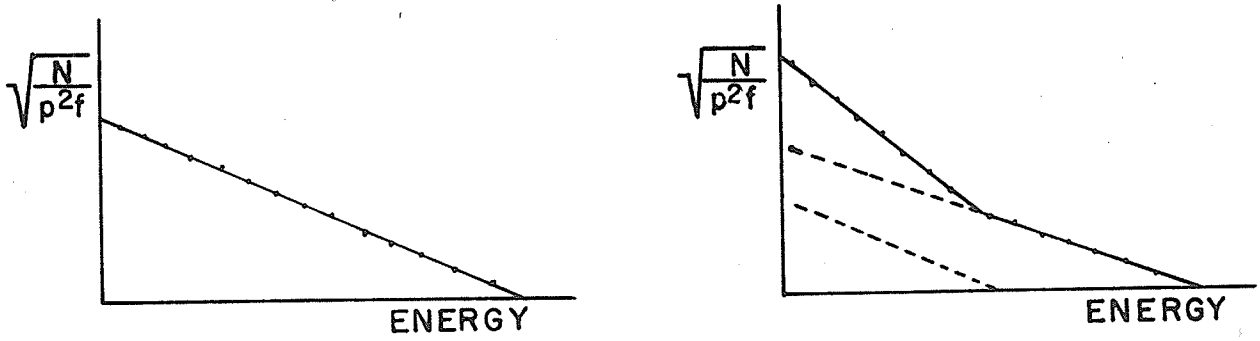

C: FERMI PLOT FOR ONE β FEED

FERMI PLOT FOR TWO β FEEDS

Fig. 1

by the relation

$$P(p)dp = T(p)\frac{dn}{dE_\beta}^{(2)} \qquad \ldots (I - 3)$$

Here P(p)dp is the probability that a β-particle will be emitted with momentum in the range p to p + dp, T(p) is the nuclear transition probability and $\frac{dn}{dE_\beta}$ is the energy density of final states which represents the possible number of oscillatory modes per unit volume of the β-particle radiation field. In order to calculate $\frac{dn}{dE_\beta}$, box normalization is used to obtain the quantum conditions for the radiation field. A method devised by Fermi[2] gives the energy density of final states as

$$\frac{dn}{dE_\beta} = \frac{(4\pi)^2 p^2 (E_{max} - E_\beta)^2 dp}{c^3 h^6} \qquad \ldots (I - 4)$$

Here p = beta particle momentum, E_{max} = maximum energy available for the transition, and E_β = the beta particle energy. The nuclear transition probability T(p) can be written as

$$T(p) = \left| \int_{space} \psi_f^* H \psi_i \, d\tau \right|^2$$

Here ψ_i is the initial nuclear wave function, ψ_f is the final nuclear wavefunction and H is a Hamiltonian for the system.

Fermi chose H to be of the form

$$H = g\phi_\beta\phi \qquad \ldots \quad (I-5)$$

Here g measures the strength of the interaction and is thus a coupling constant while ϕ_β and ϕ are time independent wavefunctions of the beta particle and the neutrino respectively. Since the interaction between the neutrino and the β field is very weak, it is possible to choose ϕ a free particle plane wavefunction, $\phi = e^{i\underline{q}\cdot\underline{r}}$, where $\underline{q}$ is the propagation vector for the neutrino and $\underline{r}$ is the position vector with respect to the nucleus. If Coulomb effects of the nucleus on the emitted β-particle are ignored then $\phi_\beta = e^{i\underline{k}\cdot\underline{r}}$, where $\underline{k}$ is the propagation vector for the β-particle. So the momentum distribution takes the form,

$$P(p)dp = g^2\left|\int\psi_f^{+}\,i\psi_f\,\exp.\left[i(\underline{k}+\underline{q})\cdot\underline{r}\right]d\tau\right|^2\frac{dn}{dE_\beta} \qquad (I-6)$$

An expansion of the exponential in a Taylor series yields

$$\exp.\left[i(\underline{k}+\underline{q})\cdot\underline{r}\right] = 1 + i(\underline{k}+\underline{q})\cdot\underline{r} - \frac{\left[(\underline{k}+\underline{q})\cdot\underline{r}\right]^2}{2\,!} + - - - \qquad (I-7)$$

The wave functions ψ_i and ψ_f vanish rapidly outside the nucleus so that integration over r is taken from zero to the nuclear radius. In this region $(\underline{k}+\underline{q})\cdot\underline{r}$ and succeeding terms are small for transition energies less than 1 Mev. Using this approximation T(p) takes the form

$$T(p) = \frac{2\pi}{\hbar}g^2\left|\int\psi_i^{+}\psi_f\,d\tau\right|^2 \qquad \ldots \quad (I-8)$$

or

$$T(p) = \frac{2\pi}{\hbar}g^2\,|M|^2 \qquad \ldots \quad (I-9)$$

where $|M|^2$ is a constant and $\hbar = h/2\pi$. Substituting (I -4) and (I - 9) into (I - 3) gives

$$P(p)dp = \frac{g^2|M|^2}{2\pi^3 c^3 \hbar^7} (E_{max} - E_\beta)^2 p^2 dp \quad . \quad . \quad . \quad (I\text{-}10)$$

This is true only for high energies, since at low energies where Coulomb effects arise, φ_β can no longer be approximated by $\exp.(i\,\underline{k}\cdot\underline{r})$. To compensate for these Coulomb effects the Fermi function $f(z,p)$ is introduced so (I - 10) becomes

$$P(p)dp = \frac{g^2|M|^2}{2\pi^3 c^3 \hbar^7} f(z,p) p^2 (E_{max} - E_\beta)^2 dp \quad . \quad (I\text{-}11)$$

Rewriting (I - 11)

$$\sqrt{\frac{P(p)}{p^2 f(z,p)}} \propto (E_{max} - E_\beta). \quad . \quad . \quad . \quad (I\text{-}12)$$

This is usually converted to the form

$$\sqrt{\frac{P(p)}{\eta^2 f(z,\eta)}} \propto (\omega - \omega_o) \quad . \quad . \quad . \quad (I\text{-}13)$$

Here η and ω are momentum and energy in relativistic units, i.e. $\eta \equiv \frac{p}{m_o c}$, $\omega \equiv \frac{E}{m_o c^2}$, m_o is the electron rest mass, and c is the velocity of light.

The plot of (I - 13) yields a straight line where the left side and ω are the variables and ω_o is the intercept corresponding to the maximum energy

available in the transition. The plot of (I-13) is called a Fermi-Kurie plot and is illustrated in fig.1(c).

If a spectrum contains more than one beta feed, the Fermi plot will reveal two or more straight line segments. The end point of the most energetic feed is found from the intercept on the energy axis. The total feed can be reconstructed by extrapolating the line segment back to the vertical axis as shown by the dashed line in fig.1(c). If this contribution to the total spectrum is subtracted, the end point energy of the second most energetic β-feed can be determined and its momentum distribution constructed. The process is repeated until all the partial spectra are found. The relative beta partial intensities can be determined from the component parts so constructed.

If only the first term 1 is retained as an approximation to the exponential in the expansion of exp.(i $\underline{k}\cdot\underline{r}$), this corresponds to an "allowed" transition. If the resulting value of the matrix element $|M|$ becomes vanishingly small, higher orders in r must be retained and then the resulting Fermi plot may be non-linear. This corresponds to a "forbidden" transition and the

highest retained order of r indicates the degree of forbiddeness for the transition.

Taking forbidden transitions into account, the right hand side of (I - 13) must include an energy dependent factor $C_n(\omega)$ known as the shape factor, where n is the degree of forbiddeness. For an allowed shape n=0 and $C_o(\omega) \equiv L_o$. This is nearly constant, but for precise work should be taken into account.

The orbital electrons surrounding the nucleus affect the nuclear field so that the Fermi function must be reduced for β^- emission and increased for β^+ emission. This screening correction S also appears on the right side of (I - 13). Both L_o[3] and S[4] have been extensively tabulated.

The final expression for the momentum distribution, taking all the corrections into account, is of the form

$$P(\eta)d\eta = \eta^2 f(z,\eta)(\omega - \omega_o)\, C_n(\omega)\, S\, \frac{dn}{dE_\beta}\, d\eta \qquad \ldots (I - 14)$$

Experimentally, the counting rate (C.R.) is a measure of $P(\eta)d\eta$. In a fixed geometry counter like the one used, the momentum interval accepted at the detector varies directly with the momentum setting. Thus N, the normalized counting rate $\left(\frac{\text{C.R.}}{\text{momentum}}\right)$, corresponds to a constant momentum interval accepted by the detector. N replaces $P(\eta)d\eta$ in the analysis.

(2) Internal Conversion

When a nucleus is in an excited state (the excitation energy being insufficient for the emission of nuclear particles), the de-excitation will proceed predominantly by one of two competing mechanisms. Either a γ-ray will be emitted or the nuclear excitation energy will be transferred to one of the orbital electrons resulting in the ejection from the atom of this electron. The energy of the ejected electron is equal to $E_\gamma - E_K$, $E_\gamma - E_{L_1}$, $E_\gamma - E_{L_{11}}$, - - - etc. depending on whether it is emitted from the K, L_1, L_{11}, - - - orbit. The process is called internal conversion and the branching ratio giving the number of conversion electrons (Nce) to the number of photons (N_γ) is the internal conversion coefficient α. That is

$$\alpha = \frac{Nce}{N_\gamma}$$

Depending whether the electron comes from the K, L_1, L_{11}, - - - etc. orbit, the conversion coefficient is termed α_K, α_{L_1}, $\alpha_{L_{11}}$ - - - etc. Thus

$$\alpha_K = \frac{\text{number of K-conversion electrons}}{\text{number of gamma rays}}$$

There are two exceptions to the de-excitation modes described. In one, the nuclear transition is

accompanied by an electron-positron pair. This requires an excitation energy greater than $2m_0c^2$(1.02 Mev.). The other exception arises when both initial and final states have zero angular momentum. Then, due to a selection rule governing electromagnetic transitions, only conversion electrons or pair production can occur. Photon emission is absolutely forbidden.

The peak to beta spectrum (P.B.S.) technique of determining the conversion coefficient involves the determination of N_γ in terms of the β-momentum continuum. The α_K conversion coefficient is obtained from the following relation:-

$$\alpha_K = \frac{\text{No. of K-conversion electrons}}{\text{No. of corresponding gamma rays}}$$

$$= \frac{\dfrac{\text{No. of K-conversion electrons}}{\text{Total no. of transitions}}}{\dfrac{\text{No. of corresponding gamma rays}}{\text{Total no. of transitions}}} \qquad \text{(I - 15)}$$

But the denominator equals the absolute gamma ray intensity, so

$$\alpha_K = \frac{\dfrac{\text{area of K line}}{\text{area of } \beta\text{-continuum}}}{\text{absolute } \gamma\text{-ray intensity.}}$$

accompanied by an electron-positron pair. This requires an excitation energy greater than $2m_0c^2$(1.02 Mev.). The other exception arises when both initial and final states have zero angular momentum. Then, due to a selection rule governing electromagnetic transitions, only conversion electrons or pair production can occur. Photon emission is absolutely forbidden.

The peak to beta spectrum (P.B.S.) technique of determining the conversion coefficient involves the determination of N_γ in terms of the β-momentum continuum. The α_K conversion coefficient is obtained from the following relation:-

$$\alpha_K = \frac{\text{No. of K-conversion electrons}}{\text{No. of corresponding gamma rays}}$$

$$= \frac{\dfrac{\text{No. of K-conversion electrons}}{\text{Total no. of transitions}}}{\dfrac{\text{No. of corresponding gamma rays}}{\text{Total no. of transitions}}} \qquad \text{(I - 15)}$$

But the denominator equals the absolute gamma ray intensity, so

$$\alpha_K = \frac{\dfrac{\text{area of K line}}{\text{area of } \beta\text{-continuum}}}{\text{absolute } \gamma\text{-ray intensity.}}$$

The gamma ray intensity is obtained from measurements taken on a curved crystal spectrometer or by gamma ray shape analysis of the spectrum obtained using a scintillation counter. The present work used this latter method. It will be described in (V - 4).

The areas are determined from the momentum spectrum obtained using the β-ray spectrometer. The K-conversion coefficient depends, among other things, on the multipolarity and the electric or magnetic character of the transition. Thus a comparison of the experimental conversion coefficient with tabulated theoretical values[5,6] serves to identify the character of the transition.

Chapter II

THE INTERMEDIATE IMAGE SPECTROMETER

Introduction:

Since beta particles are charged, they are deflected in a magnetic field. The trajectory of each particle in this field is dependent on its momentum, so that an instrument with variable magnetic field can be used to obtain the momentum distribution of β -particles emitted from a radioactive source.

The magnetic analyzer is called a β-ray spectrometer and was first designed and used by V. Baeyer and Hahn[7]. Their original unit was a flat spectrograph and had no focusing ability. Since then several different types of spectrometers have been developed including the Intermediate-Image Spectrometer, so called because of its method of focusing.

The Siegbahn-Slatis spectrometer (fig.2) used throughout this work and built commercially by LKB-Produkter Fabriksaktiebolag of Sweden is the end result of numerous refinements made on the original intermediate-image instrument.

The magnet and pole pieces have been especially designed to give an axially non-symmetric

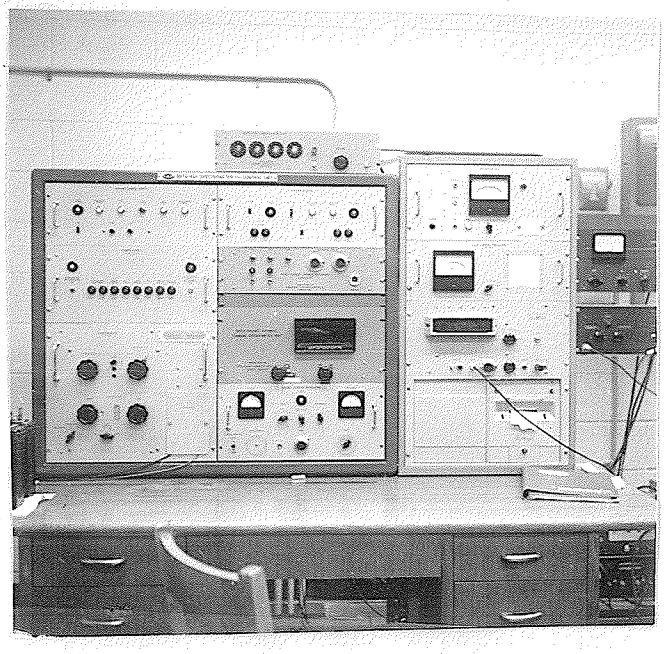

THE CONTROL CONSOLE

THE SPECTROMETER TANK

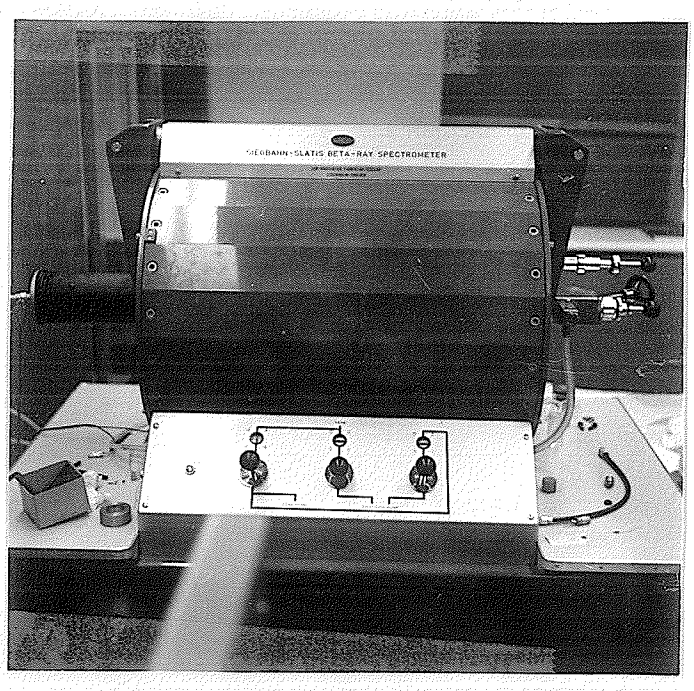

Fig. 2

magnetic field. The field is symmetric perpendicular to the spectrometer axis fig.3(1), but varies in strength along the axis from high at either end to lower in the center. The field is non-uniform so that electrons leaving the source reach the detector along helical paths whose longitudinal cross-section is shown in fig.3(2). The maximum β -particle energy that can be focused in this way is about 7.2 Mev.

The field gradient set up in the spectrometer by the coil placement is such as to give maximum transmission. Transmission is defined as the percentage of monokinetic electrons leaving a source which arrive at the counter. If δp is the spread in momentum at half-height of a conversion line profile for the momentum setting p, the resolution of the spectrometer is the ratio $\delta p/p$ expressed as a percentage.

The intermediate-image spectrometer has a considerably larger transmission coefficient than most other spectrometers, with a moderate 0.3 - 2.5 % resolution as well. Thus it is ideally suited for investigation of weak sources or for beta-gamma coincidence work where high counting rates are essential.

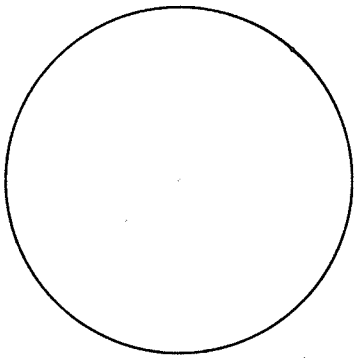

A CROSS SECTION OF β-PARTICLE ORBITS:

(1) PERPENDICULAR TO THE SPECTROMETER AXIS

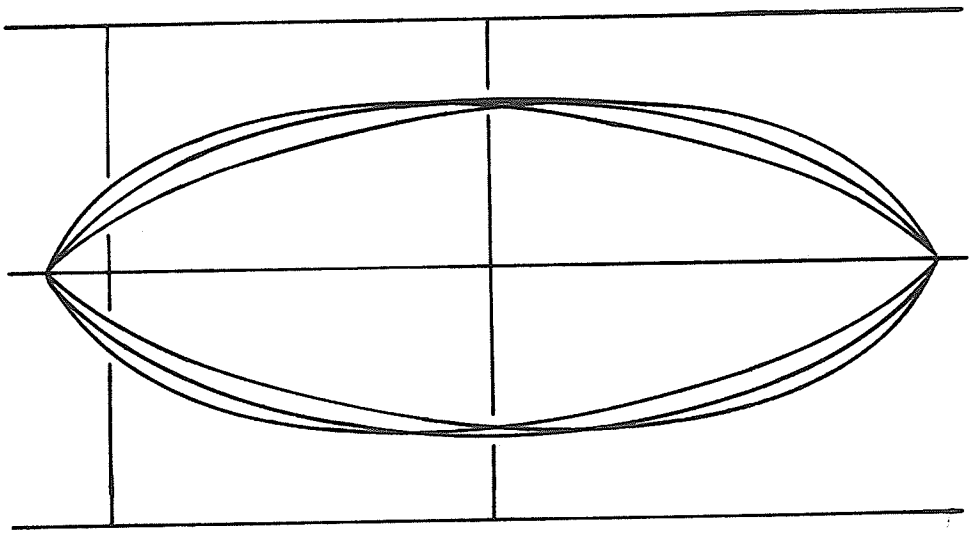

(2) PARALLEL TO THE SPECTROMETER AXIS

Fig. 3

(1) Spectrometer Chamber

The instrument is illustrated schematically in fig.4. The cylindrically symmetric chamber is 550 mm. from source to detector and about 260 mm. in diameter. The magnet consists of a number of hollow brass coils which are arranged coaxially within a cylindrical jacket and appropriately positioned with fiber spacers to produce the right focusing field gradient. The electron trajectories are defined by an annular slit located in front of the source, and a baffle system located midway between the source and detector. The slit nearest the source is referred to as the entrance window while the central baffle is called the exit slit.

The entrance window consists of a circular aluminum ring, and a coaxial circular plate located slightly further from the source. An angle of 35° is bevelled on their transmitting edge, and they are both attached to a shaft which projects outside the pole-piece. The distance between the inner plate and the outside ring can be varied from 0 to 30 mm. by rotating the shaft which is equipped with a micrometer scale. The whole ensemble can then be moved closer to or

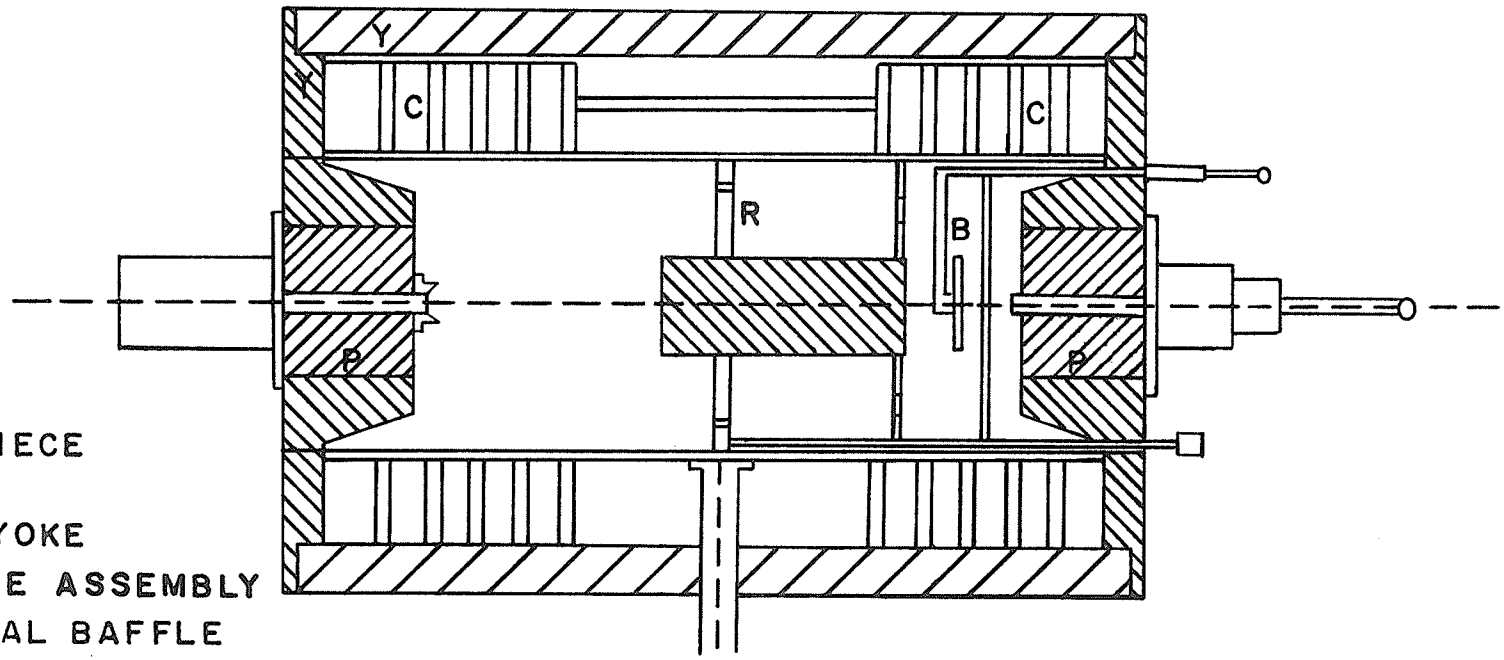

LEGEND

P POLEPIECE
C COILS
Y IRON YOKE
B BAFFLE ASSEMBLY
R CENTRAL BAFFLE

Fig.4 THE SPECTROMETER CHAMBER

farther from the inner face of the pole piece, by moving the supporting shaft parallel to the spectrometer axis. This position is again indicated by a scale inscribed on the shaft.

The exit slit (central baffle) consists of an outer circular aluminum ring of inner diameter 180 mm., and an inner circular brass plate which is coaxial and coplanar with the ring. The inner plate diameter is variable in much the same manner as a camera iris diaphragm and allows the annular slit width to vary from 0 to 10 mm. This is accomplished by means of a shaft equipped with a dial which projects through the pole-piece. The central baffle is held in place by means of an aluminum and brass framework which supports it along with a lead cylinder 10 cms. in diameter and 25 cms. in length.

The entrance window largely controls the transmission of the instrument and once optimized is then untouched. The central baffle determines the momentum resolution and the lead cylinder, which is coaxial with the spectrometer axis, prevents gamma radiation from reaching the detector.

Sources are inserted into the spectrometer chamber through a hole drilled along the axis of the pole-piece. The source holder fig.5(a) consists of a stainless steel shaft attached to one end of a stainless steel reinforced aluminum cylinder, whose open end is machined to receive an aluminum source ring. The source can be positioned along the spectrometer axis by varying the distance it is inserted through the pole-piece. Once the position is found where maximum counting rate at the detector occurs, a locking screw is set on the shaft of the holder to retain this position.

(2) The Vacuum System:

The chamber is evacuated by means of a conventional rotary and oil diffusion pump combination as shown in fig.6. The spectrometer chamber is evacuated through V_1 by the rotary pump during the roughing stage. This pump then acts as backing for the diffusion pump when valve V_3 is open. During normal operating conditions, V_1 is closed and V_2 and V_3 are locked in an open position by means of energized relays. If for any reason one of the several safety devices on the spectrometer proper is tripped, the relays are de-energized

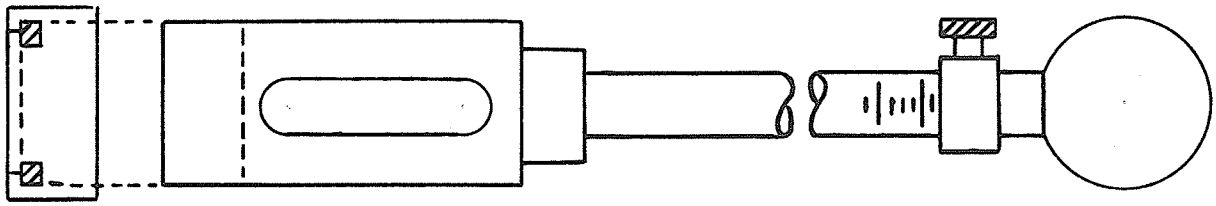

(a) THE SOURCE HOLDER

(b) THE DETECTOR

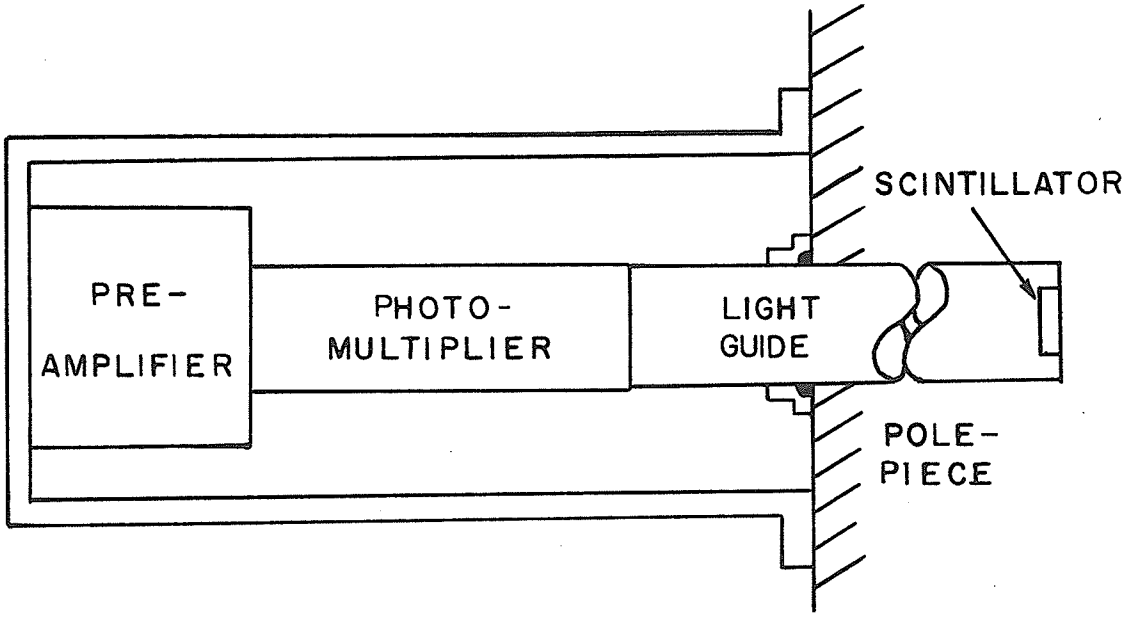

Fig.5

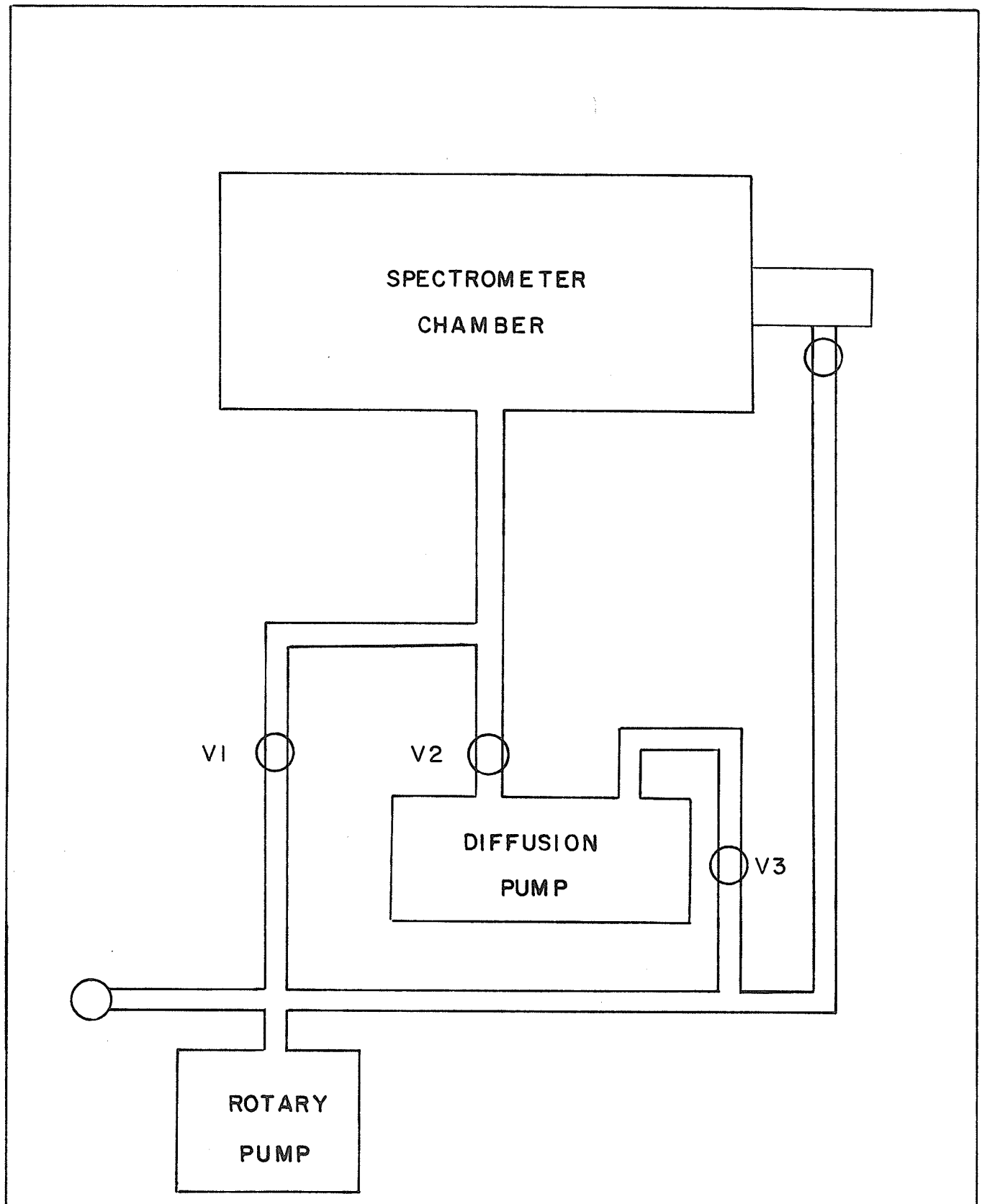

Fig.6 THE VACUUM SYSTEM

and the pump valves are closed by heavy springs in order to protect the diffusion pumps in the event of a vacuum leak.

To prevent oxidation of the hot diffusion pump oil, valve V_2 will not remain open unless a sufficiently low vacuum pressure of 100 microns is reached. The control panel contains a vacuum gauge which can be used to indicate the pressure in the fore vacuum pump, the diffusion pump, or the spectrometer tank.

(3) Current Regulation:

The current through the coils is measured by the potential developed across a 0.002Ω water cooled oil-immersed manganin resistor. A current of 1 ampere through the resistor corresponds to 2 millivolts (mv.) across it.

The voltage developed across the standard resistor is fed to a precision potentiometer where it is compared against a continuously variable reference source. The error between the two is amplified by a D.C. amplifier and fed through the exciter windings of the D.C. generator which supplies current to the spectrometer coils. The generator output changes so

that the error signal is reduced and a balanced condition is rapidly obtained. Thus the potential drop across the standard resistor is constantly corrected to equal that of the reference source. Error signals too large to be handled by the D.C. amplifier activate a motor driven potentiometer which in turn regulates the generator output through a third exciter winding.

(4) Detection:

The control console is pictured in fig.2. It consists of the main spectrometer controls, plus recently acquired automation equipment described by Konopasek and Connor[8]. Particle detection is accomplished using either a Geiger-Müller counter or a scintillation counter. The spectrometer was originally provided with a Geiger counter by the manufacturers but because of the long dead time of the counter (approximately 250μseconds), a scintillation counter (dead time approximately 1μ-second) was fitted during the process of automating the spectrometer. The scintillator is a piece of NE102[+] scintillating plastic which is recessed into the face

[+] Available from Nuclear Enterprises, 550 Berry St., Winnipeg, Manitoba.

of a lucite light pipe optically coupled with Dow Corning Vacuum grease, to a low noise E.M.I. 1" photo-multiplier, type 9524SA. The light guide projects through the pole-piece and the scintillator is located at the focal point of the spectrometer. The photo-multiplier is completely enclosed in a mu-metal lined brass cylinder in order to shield it from any stray magnetic field which could change the gain of the photo-multiplier considerably. Power and output signal connections are made through one end of the brass cylinder which shields the photo-multiplier, while the other end is bolted to the outside of the spectrometer pole-piece and made light tight with plasticene. A block diagram of the detection apparatus is illustrated in fig.7. High tension to the photo-multiplier is supplied by a Hamner model N401 high voltage power supply. Output pulses from the photo-multiplier are fed via a transistorized preamplifier into a T.M.C. AL-2A linear amplifier whose output is coupled to a Hewlett-Packard scaler model 521 ER. The counter is coupled to a Hewlett-Packard model 561 B digital printout recorder.

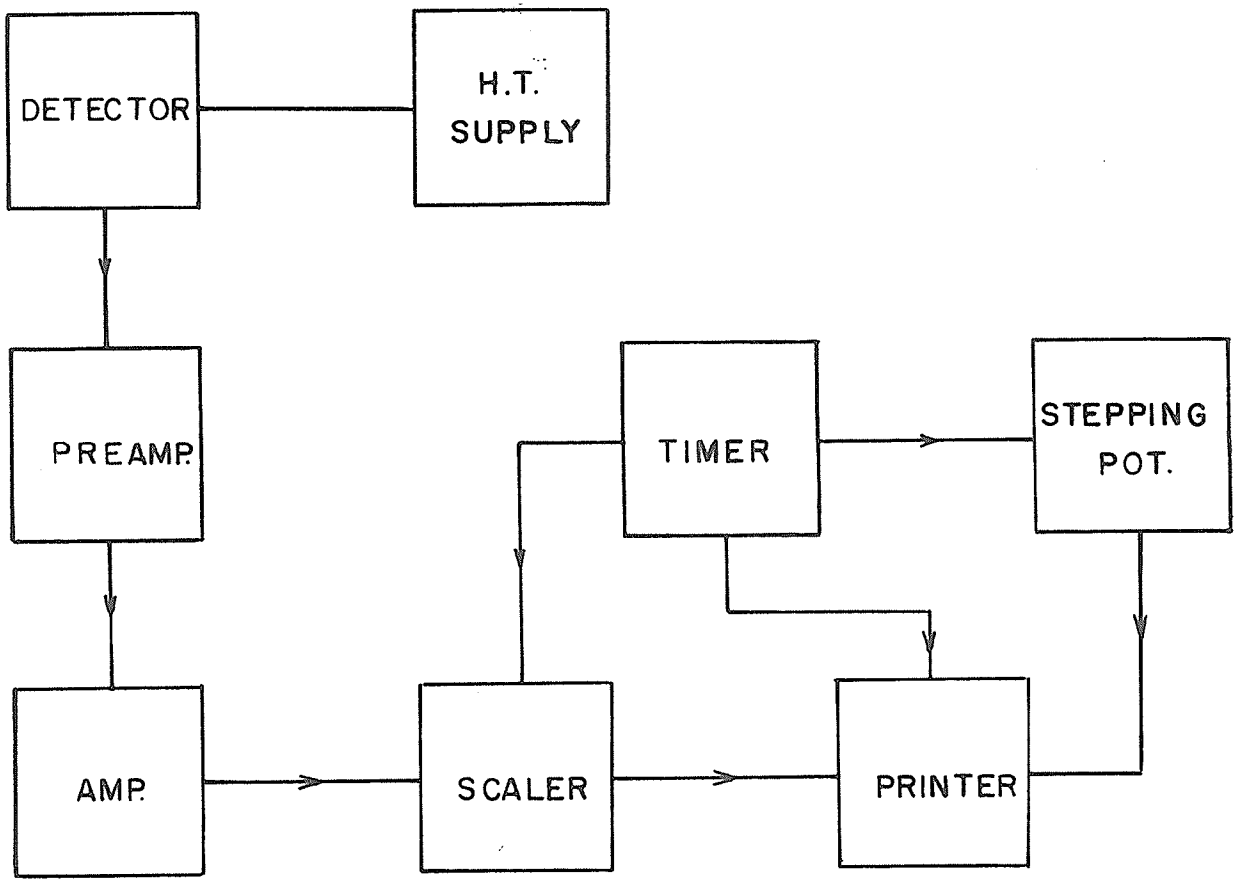

Fig.7 THE DETECTION APPARATUS

(5) Automatic Data Recording:

The stepping potentiometer is connected to a timer+ which operates on 60 c.p.s. line voltage and can be set for time intervals from 1 to 2000 seconds. At the end of the chosen time a pulse from the timer triggers the recording device which prints out the numbers appearing on the scaler and stepping potentiometer at that instant. At the same time a pulse is fed to the stepping potentiometer and advances it one unit initiating the next cycle. After 10% of the selected time period has passed the scaler receives a delayed pulse from the timing mechanism which clears it to zero. This 10% period is inserted so the generator and D.C. amplifier will have had time to become stabilized on the new current setting. This settling down time is of the order of 1 second. In order to increase the stepping rate by a factor of two, an auxilliary mechanism was incorporated which allows the stepping potentiometer to be advanced on the scaler clear pulse as well as the print pulse. Since all of the runs taken throughout this work were 500 seconds or more per point, the

+ Interscience Timer/Counter N.65

error due to the omission of the generator recovery time in this double-step position is negligible. The main advantage of the double-step unit is that it allows closer examination of conversion line spectra without readjustment of initial conditions. The run proceeds by double steps on the gross continuum until the region possessing conversion line structure is approached. The control is then switched to the "single-step" position consequently allowing twice as many observation points per selected momentum interval to be taken.

(6) The Scanning Potentiometer:

The Inter-Science automatic scanning potentiometer, provides a steppable reference voltage from zero to 1.5 volts. The voltage developed across the .002 Ω standard resistor in series with the coils is compared with this reference. The 1.5 volt power supply for the potentiometer is stabilized by two Zener diodes in parallel. These diodes are located in a temperature controlled oven to ensure that no thermal drifts in the diodes occur. The stability

is good to 1 part in 10^4. Levels for the output voltage are set with two helipots and are variable between 0 and 1.5 volts. The voltage between the two helipots is then divided into 9999 parts across the scanning potentiometer. A reading of 5000 on the scanning potentiometer digital meter indicates that one half of the total difference between the two helipots is being fed to the D.C. amplifier as a reference. The figure on the meter is printed on the recorder tape next to the number of counts which have accumulated, when the print command from the timer is received.

Chapter III

SPECTROMETER PERFORMANCE

Introduction:

The functioning of the automatic equipment including the scintillation counter was tested to be certain of proper performance. The well known conversion lines in Thorium (B + C) were used to check the linearity of the momentum spectrum. The momenta of the strongly converted transitions in Thorium B have been accurately determined. A plot of momentum versus millivolts for the observed conversion lines indicates the linearity of the instrument. At the same time, the spectrometer is calibrated, that is, since the millivolt reading is a constant times the β -particle momentum, the calibration of the spectrometer implies determination of this constant.

To detect any possible instrumental distortion of the shape of a β -spectrum, the Sodium-24 (Na^{24}) isotope, which is known to have a single high energy allowed β -transition, was investigated.

(1) The Thorium F Line Calibration:

Thorium sources are obtained from a "pot"

containing radio-thorium which decays with a 1.9 year half-life by way of ThX to gaseous Thoron. Thoron decays by α-emission to ThA with a 54 second half-life and the latter is a solid at room temperature. The process of α-emission disturbs the extra nuclear structure of the resulting ThA atoms by ionization and produces both positively and negatively charged ions which can be collected by electrostatic attraction. To prepare a calibration source, the ions are collected on the tip of a rounded aluminum needle or wire which is kept at a negative 300 volt potential. The ThA collected in this way decays by α -emission with a 0.16 second half-life to ThB. ThB in turn decays to ThC, ThC', and ThC". The ThB along with ThC, ThC' and ThC" comprises the Thorium active deposit which decays with an equilibrium half-life of 10.6 hours; that of ThB.

The source obtained in this way is only a few atoms thick and source absorption effects[9] are negligible. Although electrons of the intense conversion lines are strongly backscattered by the backing, this does not affect their shapes or positions and hence lines from such sources are suitable for calibration.

The backscattering of electrons does however, render such sources unsuitable for observations of the β-continuum. The series of intense well separated conversion lines found in the Th source made an excellent calibration since the $\beta\rho$ values of these lines have been determined by Siegbahn and Edvarson, and Lindstrom[10] to within 1 part in 10^4.

The Thorium F-line is the most intense of the many conversion lines and was used to test the functioning of the automatic equipment. Fig.(8) shows the experimental line shape of the F-line. Its momentum value in units of $\beta\rho$ is known and from the relation

$$\beta\rho = p/e = \frac{m_o c \eta}{e}$$

$$\eta = \frac{e\beta\rho}{m_o c} = \frac{\beta\rho}{1704.4} = K \times (mv.)$$

where mv. is the millivolt reading corresponding to a given $\beta\rho$ value and K is the calibration constant. Further lines in the spectrum allow a check on the value of K determined.

(2) Demagnetization Procedure:

Demagnetization of the spectrometer prior to any investigation is essential in order to remove any possible residual magnetism in the spectrometer which

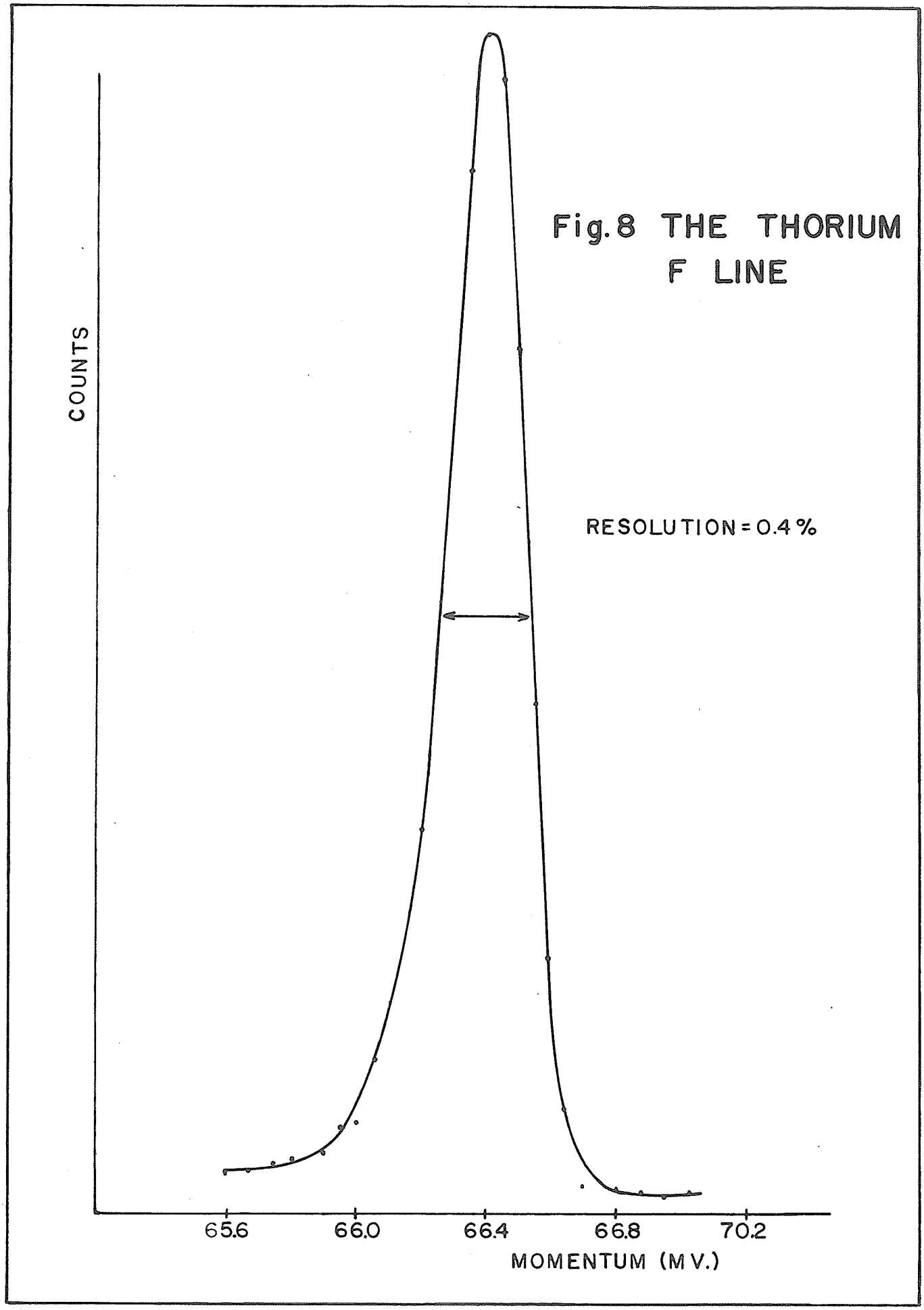

Fig. 8 THE THORIUM F LINE

could alter the momentum calibration. The current is increased to 650 amperes in the forward direction and then decreased to zero. The current is then increased to 650 amperes in the reverse direction and again decreased to zero. The cycle is repeated for successively smaller values of current until a current value of 10 amperes is reached. The process can be compared to taking the spectrometer around hysteresis current loops and in this way the demagnetization is accomplished.

(3) Distortion Investigations:

It is very important that the spectrometer does not introduce any instrumental distortion into the β-spectra. This distortion could be introduced by scattering inside the spectrometer or from source thickness or source backing effects, most of which tend to increase the number of low energy counts. In order to test for spectrometer effects a source whose spectrum is long and consists of one beta feed having the allowed shape would be desirable, the source itself being as thin and uniform as possible.

Na^{24} which decays with a half-life of 15.0

hours was chosen to check the spectrometer. Its activity is due to one beta feed which is known to yield a straight Fermi plot[11]. A shipment of Na^{24} was obtained from Oak Ridge National Laboratories, Oak Ridge Tennessee, in a solution of HCl. The material received had a specific activity of ~ 1000 millicuries per gram of Na. The source was prepared by subliming Na^{24} in vacuum onto a V.Y.N.S. backing (discussed in the next section). Visual observation showed that the quality of the source was no better than that of the Au^{198} and Au^{199} sources used throughout the experimental work. Since its spectrum is quite long, in order to sublime sufficient activity to give reasonably good statistics (~1%), enough Na^{24} material had to be sublimed to make the source quite visible.

The analysis of the data obtained for the Na^{24} yielded an end point of 1392 kev which is in good agreement with the accepted value of 1391 kev (Nuclear Data Sheets). Fig.(9) shows the Fermi plot of Na^{24}. The Fermi Plot is straight down to less than 150 kev. The small upward curvature evidenced at energies lower than this is believed to be due to source absorption. The spectrum for Na^{24} is much longer than that of

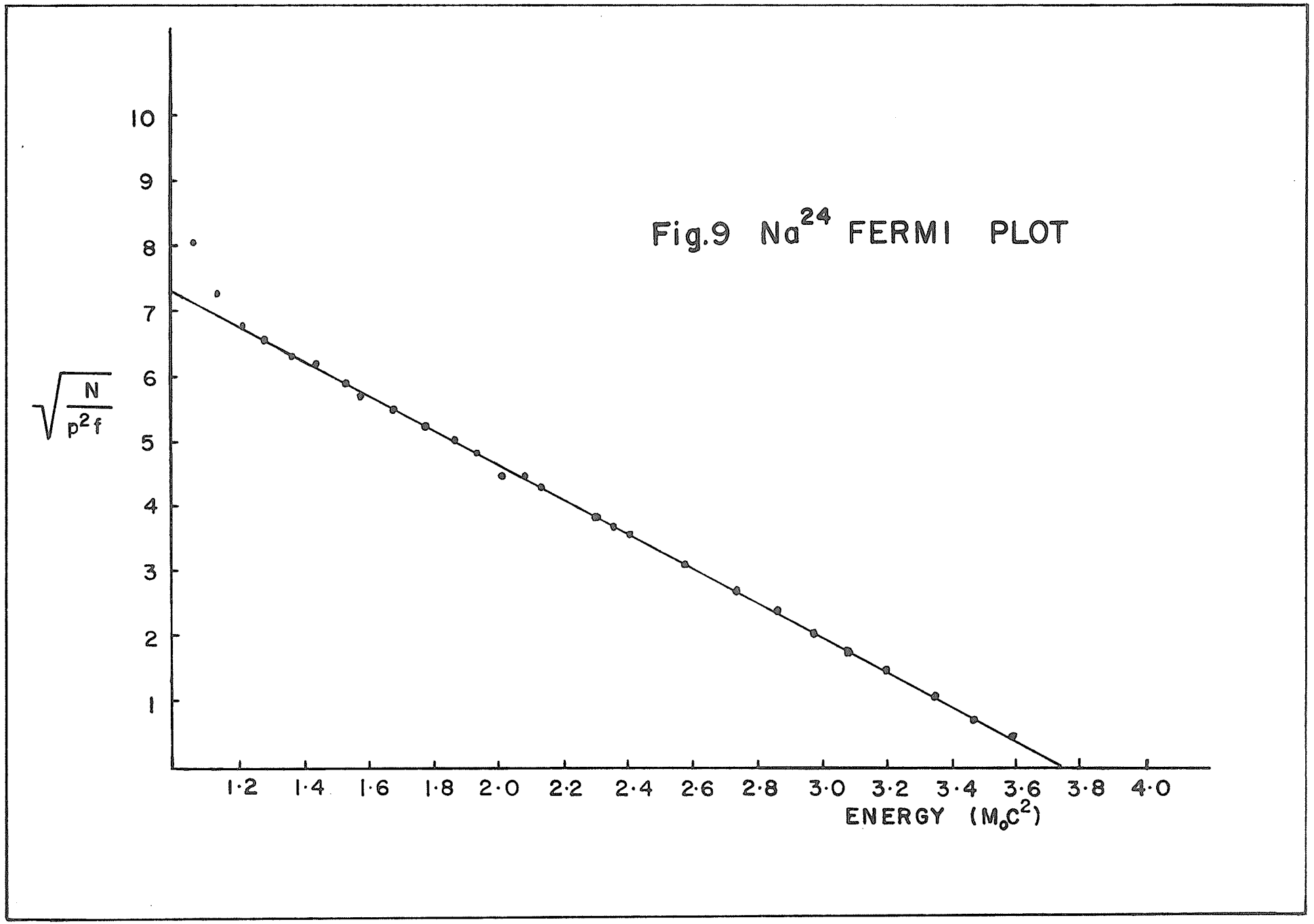
Fig.9 Na^{24} FERMI PLOT
$\sqrt{\frac{N}{p^2 f}}$
10
9
8
7
6
5
4
3
2
1
1·2
1·4
1·6
1·8
2·0
2·2
2·4
2·6
2·8
3·0
3·2
3·4
3·6
3·8
4·0
ENERGY (M_0C^2)

either Au^{198} (end point 960 kev.) or Au^{199} (end point 460 kev.) so that absorption and scattering effects would be much more noticeable in the case of Na^{24}. The conclusion was that the spectrometer was reliable for precise investigations of the spectra of Au^{198} and Au^{199}.

Chapter IV

SOURCE PREPARATION

Introduction:

The method of source preparation used is next in importance to absence of spectrometer distortion for the precise investigation of β-ray spectra. Ideally the source should be strong enough so that the statistical accuracy in the number of counts ($\frac{\Delta N}{N}$) is 1% or better over the entire spectrum. The source should be invisible (massless) and supported by a massless conducting backing. Source thickness produces both absorption and backscattering in varying degrees, depending on the thickness of the source. Source backings produce backscatter and for this reason are usually made from thin materials with a low atomic number. Both source absorption and backscattering will distort the spectral shape by giving an excess number of low energy particles such that an analysis of this spectrum will yield erroneous results.

(1) Source Backing:

Since source backings are to be as thin and weightless as possible, organic compounds and aluminum foils are usually used. Organic compounds such as

zapon, collodion, nylon, formvar, and V.Y.N.S. resin find wide application. They have thicknesses corresponding to surface densities less than or equal to 20 $\mu g/cm^2$. In the past, most workers used drop sources deposited on one or another of these organic films. Each film is made conducting so as to prevent charging of the source as the beta particles are emitted. Douglas[12] reported shifts in energy of as much as 19 kev for the 46.9 kev conversion line in the spectrum of Lu^{177} by using an ungrounded nylon backed source. Thus evaporation of gold or aluminum metal onto these films is essential. V.Y.N.S. has the most desirable properties of all the organic compounds. It is strong, has excellent chemical resistance, is easily handled, and may be obtained in thicknesses varying from 1 to 10 $\mu g/cm^2$.

Aluminum foil is also used for source backings mainly because of its far superior tolerance to heat. The thickness is much greater however, and varies from about 200 $\mu g/cm^2$ to larger values. It has the advantage that it is already conducting but work done in this department indicates that when it is used, even with the thickness mentioned, backscattering is

always present. All the sources used in this investigation were deposited on V.Y.N.S. backings.

(2) Preparation of V.Y.N.S. Source Backings:

V.Y.N.S. resin (a polyvinylchloride acetate copolymer) is commercially available from Shawinigan Chemicals Ltd. (Montreal, Canada). Its mechanical strength and chemical resistance make it a very good source backing material. Green, (previously of this department), has devised a method for preparing very thin V.Y.N.S. films and this method was used throughout. V.Y.N.S. is dissolved in 2 to 3 times its volume of cyclohexanone. A small amount of the solution is spread evenly along the edge of a clean glass plate. The coated edge is carefully brought in contact with the surface of still water where surface tension spreads the solution evenly over the water. The cyclohexanone evaporates leaving a thin V.Y.N.S. film. This is then mounted on one face of a circular source ring after being removed from the water with a small wire hoop. The hoop is allowed to pass under the film in the water and is then raised until its circumference is totally in contact with the film. A small paint

brush is dipped into cyclohexanone and used to dissolve a ring in the film outside the hoop's circumference. By sliding and raising the hoop to one side, the V.Y.N.S. film is lifted from the water. The hoop is then placed concentrically over the source ring and brought down until contact between the ring and film is made. The paint brush is again employed to "cut" the film free from the hoop leaving it taut over the upper face of the source ring. Any water which is clinging to the film is allowed to evaporate. Then the ring and film are ready to be coated with metallic gold to render the film conducting.

(3) Gold Evaporation onto V.Y.N.S. Backings:

The vacuum evaporation of metallic gold onto V.Y.N.S. is accomplished in the Edward "Speedivac" model 12EA620 evaporation unit. The V.Y.N.S. coated rings, described in the last section, are put inside the bell jar of the unit at a height of about 5 inches above a molybdenum filament.

A small piece of metallic gold is deposited on the filament and when a pressure of 0.2 microns is reached inside the jar, current is passed through the

filament by a variac control. Current is increased until the metallic gold sublimes. The process must be carried out quickly as the V.Y.N.S. films are easily destroyed by too much heat from the filament.

(4) Vacuum Deposition of Radioactive Source Material:

Work done in this department on Cs^{134} (13) showed that sources obtained by drying a small drop of solution onto V.Y.N.S. backing were not of sufficiently good quality for precise investigations. These sources are very inhomogeneous and upon close examination were found to consist of aggregates of CsCl micro-crystals. This crystalline structure causes a strong absorption of low energy β-particles and a loss of energy for β-particles in general. Thus it was decided that a vacuum sublimation process would be very desirable since crystalline structure is avoided and the sources are as uniform and as thin as possible.

The evaporation chamber shown in Fig. 10 is evacuated by the usual rotary-diffusion pump ensemble, the rotary pump acting as a backing pump for the diffusion pump, as well as a separate roughing

LEGEND

A HOLDER
B MASK
C SPACER
D SOURCE RING
E FILAMENT

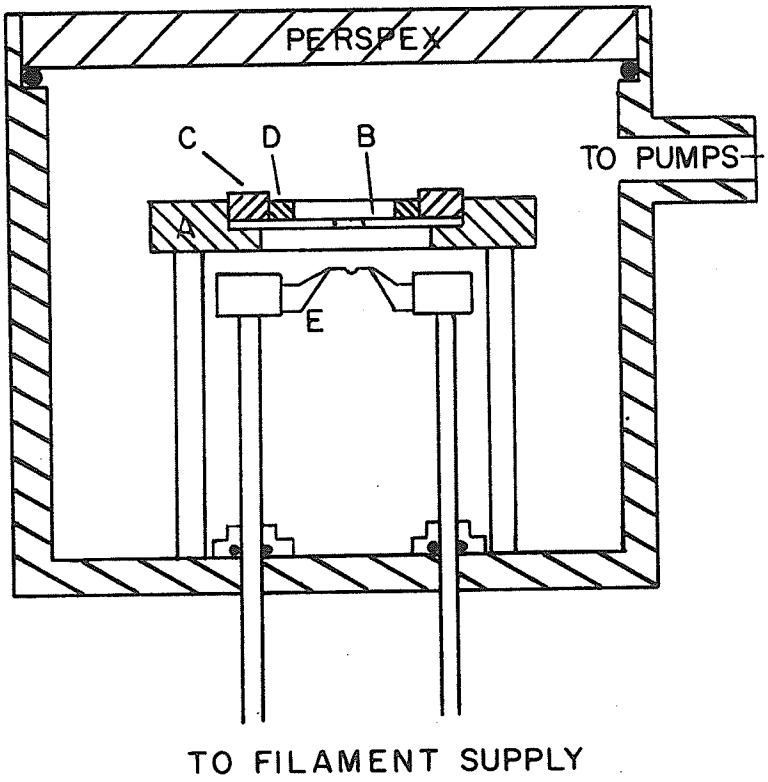

VACUUM SUBLIMATION CHAMBER

Fig. 10

pump through an alternate valve inlet.

The lid of the chamber consists of clear perspex which, when placed on top of an O -ring, forms an airtight window for the chamber. The tantalum filament used in the evaporation process is clamped in place across two studs projecting through and insulated from the bottom of the chamber. The ring supporting the V.Y.N.S. film is located over the filament by a mask. The mask isolates the V.Y.N.S. from the filament except for a circular opening in its center. The sublimed activity passes through this hole and is deposited on the V.Y.N.S. film. The mask assembly is supported by three rods which are screwed into the chamber floor.

Power connections to the filament are made outside the chamber on the two filament locating studs. The filament supply is obtained from the output of a 10 to 1 step-down power transformer. The transformer primary is fed from a variac, which derives 115 volt, 60 cycle A.C. from a wall outlet through a relay. The relay is controlled by a Schmitt trigger circuit (Fig. 11) which allows both the "off" and the "on" time at the filament to be varied

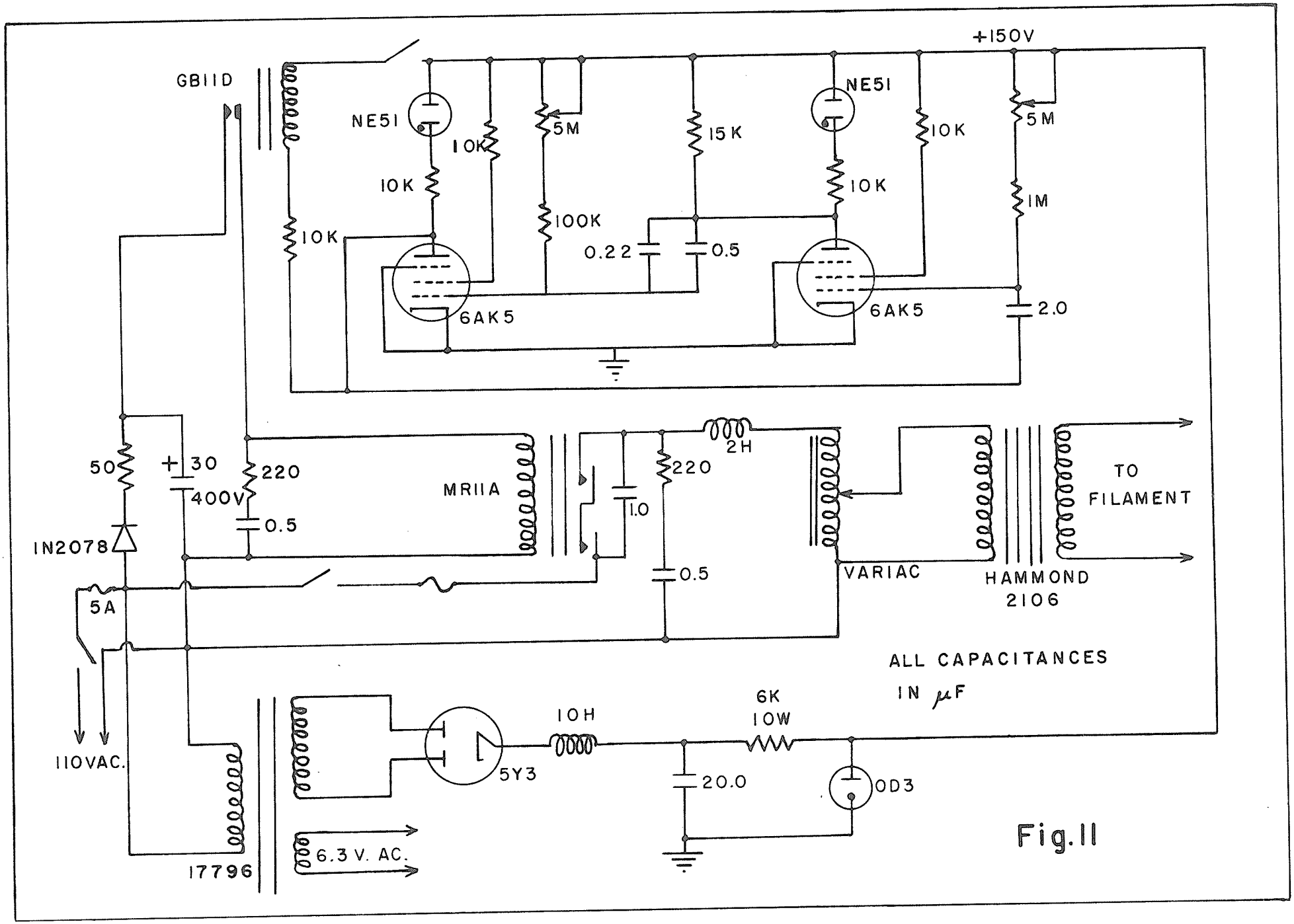
+150V
GB11D
NE51
10K
10K
10K
5M
100K
15K
0.22
0.5
6AK5
NE51
10K
10K
5M
1M
6AK5
2.0
50
+30
400V
220
0.5
IN2078
5A
MR11A
1.0
220
0.5
2H
VARIAC
TO
FILAMENT
HAMMOND
2106
ALL CAPACITANCES
IN μF
110VAC.
17796
6.3 V. AC.
5Y3
10H
6K
10W
20.0
OD3

Fig.11

depending on the settings chosen. The variac enables the transformer to be varied from 0 - 130 volts A.C.

In preparing a typical source, the perspex cover and the mask assembly are removed from the evaporation chamber. The filament is properly positioned and a dimple, which has previously been formed in the middle of it, is filled with radioactive solution using a hypodermic syringe. The solution is gently heated with a heat lamp to speed the evaporation of the liquid. After several drops have been dried in the dimple, the source holder is repositioned on its three supporting studs. The dimple in the filament should now be directly under the middle of the V.Y.N.S surface. The mask which shields the V.Y.N.S. from the filament contains a central hole 2 mm. in diameter.

Once the source holder is positioned, the perspex cover is replaced and evacuation of the chamber is begun using the rotary pump only. After most of the air has been evacuated from the chamber, the diffusion pump is inserted between the chamber and the rotary pump by a valve arrangement. The rotary pump now acts as backing for the diffusion pump. When the chamber is evacuated sufficiently, the power to the

Schmitt trigger circuit is turned on, and the filament is heated by increasing the variac reading from zero.

The filament supply is generally pulsed at a repetition rate of about 1 second on, 1 second off, since in this way more precise control of the filament temperature is maintainable. When the filament becomes sufficiently hot to sublime the radioactive source material, part of the material is collected on the V.Y.N.S. directly above the dimple. The collection efficiency is not better than 2%, with most of the activity going on the mask and a sizable fraction of the whole remaining unsublimed. However, the source obtained in this way is virtually unsurpassable with regards to uniformity and thinness.

Chapter V

PRESENT INVESTIGATIONS

Introduction:

Both Au^{198} and Au^{199} have been investigated many times and most of their characteristics are well established. The main features of the decay schemes are illustrated in Fig.12. From the spins and parities listed for the Au^{198} it is evident that the intense 960 kev. β-feed is a 1st forbidden transition ($\Delta I = 1$, and $\Delta \pi$ = yes). As such, it may exhibit either an allowed shape or non-allowed shape, depending on the strengths of the various nucleon interactions.

For some time the transition was thought to exhibit the allowed shape, but in the last decade, as instrumentation has become more precise, several investigators[14-17] have reported deviations from linearity. This non-linearity is most pronounced in the low energy portion of the spectrum. Since there seems to be some disagreement as to the extent of the non-linearity, it was decided that a re-examination of the spectrum might help resolve the situation.

The first excited state of the Au^{198} daughter nucleus (Hg^{198}) appears at 412 kev. It is populated

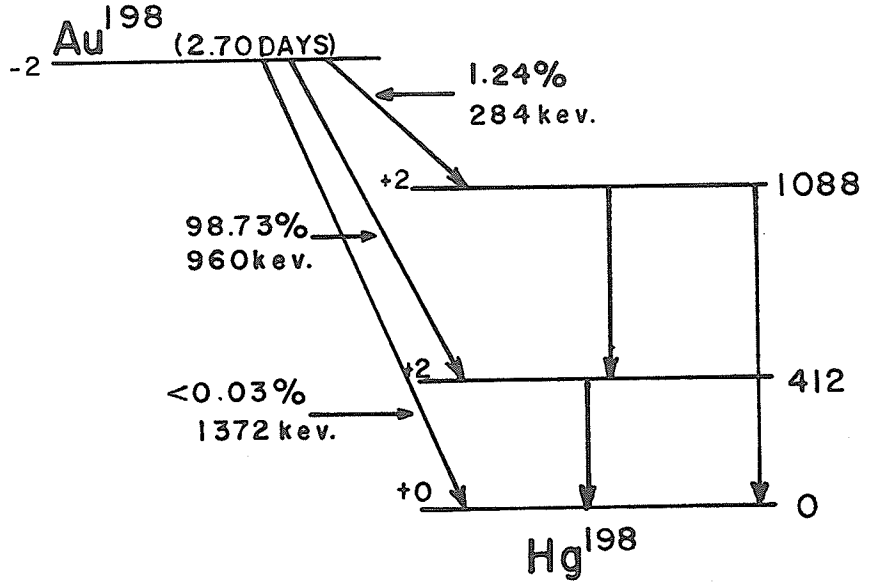

(a) Au^{198} DECAY SCHEME

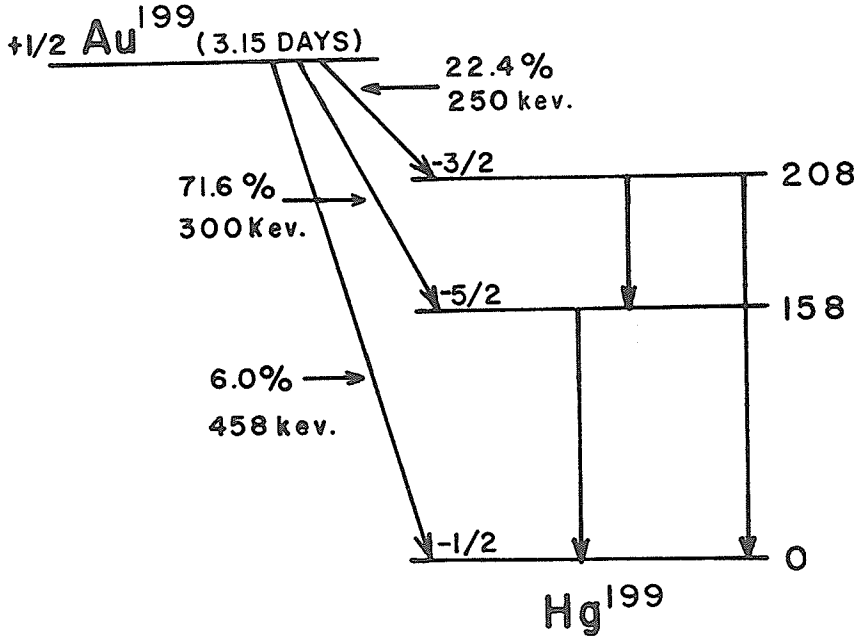

(b) Au^{199} DECAY SCHEME

Fig. 12

by the 960 kev. β -transition along with the majority of the transitions from the upper excited level appearing at 1088 kev. Thus its de-excitation represents almost 100% of all the decay events. The spin and parity of the 412 kev. level are known to be 2^+ and the subsequent transition to the 0^+ ground state must be pure electric quadrupole (E2).

Au^{198}, with atomic number Z = 80, occurs in a region of the periodic table where the K-conversion coefficient for E2 radiation is in general agreement with theoretical predictions. In the case of Au^{198} however, the experimentally determined 412 kev. K-conversion coefficient has varied from agreement with theory to results which are as much as 30% low. The majority of reported coefficients are about 15% low.

Many of the coefficient determinations were made using the peak to beta spectrum (P.B.S.) technique. Since this technique involves, among other things, a precise determination of the beta continuum, the question of the linearity of the 960 kev. β -feed again arises. Thus the present determination of the spectrum shape will allow the computation of the K-conversion coefficient as well.

Au^{198} is formed by neutron capture in stable Au^{197}. Au^{198} has an enormous cross-section for slow neutron absoprtion (2.6×10^4 barns), Consequently, Au^{199} appears as a contaminant in the Au^{198}. The well-defined conversion lines in the Au^{199} decay appear superposed on the Au^{198} beta spectrum and are a means of determining the total Au^{199} contaminant. A ratio of conversion line area to total beta continuum for the Au^{199} enables a determination of the percentage Au^{199} continuum in the Au^{198} spectrum to be made. In order to establish precisely the ratios of line to continuum area for the several Au^{199} conversion lines, a separate examination of the isotope was required.

(1) Experimental Investigations:

The active materials were obtained in HCl solution from Oak Ridge National Laboratories, Oak Ridge, Tennessee. The specific activity of the solution was 35 Curies per gram for the Au^{198} and 10 Curies per gram for the Au^{199}. The sources were prepared by vacuum sublimation of the activity onto V.Y.N.S. films as described, in section (IV - 4).

The sources examined were strong enough to give an average statistical accuracy of 1% over the entire spectrum and at the same time were virtually invisible.

An estimate of total source thickness including backing was set at 20 $\mu g/cm^2$. The V.Y.N.S. is known to vary from 2 - 7 $\mu g/cm^2$ (18), the metallic gold deposit was 5 $\mu g/cm^2$, while the source deposit was calculated to be from 5 - 10 $\mu g/cm^2$ (knowing the specific activity and counting rate at the detector).

Each Au^{198} source examined remained in the spectrometer for about 60 hours, since the 220 mv. long spectrum was scanned in 1/2 mv. steps at 500 seconds per setting. Thus after one complete run the source material had decayed by almost one half-life so that in order to acquire sufficient accuracy on another run, without increase of source thickness, a new source shipment was necessary. If a second source was prepared from the old solution, too much stable salt sublimed onto the V.Y.N.S., suggesting the possibility of source absorption effects. Four Au^{198} and two Au^{199} shipments produced sources of sufficiently good quality to be analyzed.

(2) Analysis of the Data:

The data was Fermi analyzed on the Bendix G-15 computer at the University of Manitoba. For radioactive decay processes, the well-known equation $A = Ae^{-\lambda t}$ applies. Here A is the number of radioactive atoms in a sample at time $t = t_1$, and Ao is the number at $t = 0$. In order to correct the observed counting rate for source decay, normalization to constant Ao is accomplished by multiplying observed values by $e^{\lambda t}$, where t increases from point to point. At $A = Ao/2$,

$\frac{Ao}{2} = A_o e^{-\lambda \tau}$, τ = half-life. Taking natural logarithms and cancelling Ao,

$\ln 2 = \lambda \tau$ i.e. $.693 = \lambda \tau$

so λ is determined in terms of the half-life τ for the isotope in question. The Au^{198} work was corrected for source decay using $\tau = 2.70$ days, and for Au^{199}, $\tau = 3.15$ days was used.

In the Au^{198} work, the momentum calibration constant (described in section III - 1) was obtained by examining the intense 412 K-conversion line and the contaminant Au^{199} 158 L-conversion line. For Au^{199} three of the intense conversion lines were used.

In the analysis of the data, the Fermi plot was obtained using the relation

$$P(\eta)d\eta = \eta^2 fS(\omega_o - \omega)^2 C(\omega)d\eta$$

as described in section (I - 1). Here the normalized counting rate N is a measure of $P(\eta)d\eta$. The computer typed out values of millivolts (Constant x η), energy (ω), $N/\eta^2 fS$, $\sqrt{N/\eta^2 fS}$, and N for each point analyzed. Table I is a sample page.

Once the Fermi analysis was finished, the normalized spectrum and the Fermi plot could be drawn using N vs. mv., and $\sqrt{N/\eta^2 fS}$ vs. ω respectively. A diagram of the Au^{198} normalized spectrum showing the presence of the Au^{199} contaminant conversion lines is plotted in Fig. 13. The corresponding Fermi plot is shown in Fig. 14(A), with an end point energy of 960.7 kev. Run no. 2 gave 960.2 kev. To find the shape of the 960 kev. β -feed, the Au^{199} contaminant and the low energy Au^{198} β -feed must be subtracted from the original spectrum.

The shape of the Au^{199} normalized beta spectrum is shown in Fig. 15. The intense conversion lines are labelled. In order to determine the ratio of conversion line areas to total beta continuum for the Au^{199}, the

TABLE I

Millivolts	Energy	$\frac{N}{\eta^2 Sf}$	$\sqrt{\frac{N}{\eta^2 Sf}}$	N
66.4000000000	1.27977496471	34.7337839060	5.89353746964	120.977844339
66.9000000000	1.28353648534	35.8776007039	5.98979137399	126.123410024
67.4000000000	1.28731510936	31.5729942718	5.61898516387	112.026850355
67.9000000000	1.29111068660	26.8861966869	5.18519013026	96.1273237619
68.4000000000	1.29492306800	24.9284109150	4.99283595915	90.0862135547
68.9000000000	1.29875210557	26.0223243245	5.10120616369	94.8929976999
69.4000000000	1.30259765243	27.4489800034	5.23917741667	100.995995083
69.9000000000	1.30645956279	27.0565135531	5.20158759929	100.439554249
70.4100000000	1.31041541899	26.1303733830	5.11178768955	97.8758894643
70.4100000000	1.31041541899	25.5985195178	5.05949795116	95.8837376737
70.9100000000	1.31430994345	24.5842905230	4.95825478601	92.8912661092
71.4100000000	1.31822039785	23.5793308583	4.85558553168	89.8675779691
71.9100000000	1.32214664082	23.5748584713	4.85539478016	90.6239182143
72.4100000000	1.32608853214	22.8776777930	4.78306155020	88.6944061503
72.9100000000	1.33004593267	23.0582499507	4.80190066023	90.1509040257
73.4100000000	1.33401870438	23.1256945667	4.80891823248	91.1732431588
73.9100000000	1.33800671036	22.9227934614	4.78777541885	91.1252983150
74.4100000000	1.34200981480	22.9072899755	4.78615607513	91.8151529444
74.9100000000	1.34602788298	22.7668904944	4.77146628348	92.0062459215
75.4200000000	1.35014158962	22.7413954164	4.76879391632	92.7070049532
75.4200000000	1.35014158962	22.6547125559	4.75969668738	92.3536357680
75.9200000000	1.35418947817	22.2531445991	4.71732388109	91.4877250094
76.4200000000	1.35825193035	22.6024750634	4.75420603922	93.7071178600
76.9200000000	1.36232881584	22.4780548009	4.74110269884	93.9701912467
77.4200000000	1.36642000548	22.3664915879	4.72932252948	94.2788366708
77.9200000000	1.37052537115	22.0927543021	4.70029300173	93.8905374846
78.4200000000	1.37464478584	22.3092965130	4.72327180173	95.5838628415
78.9200000000	1.37877812364	22.4267873441	4.73569291067	96.8643788147
78.9200000000	1.37877812364	22.3454872150	4.72654671126	96.9952634107
79.4200000000	1.38292525970	22.2775608100	4.71991110192	96.9918061079
79.9200000000	1.38708607026	22.0029724184	4.69073260998	96.5587482430
80.4200000000	1.39126043263	21.0483901440	4.58785245447	93.0989845237
80.9200000000	1.39544822519	21.0358205344	4.58659138515	93.7767744189
81.4200000000	1.39964932739	20.8538685957	4.56660361710	93.6838451333
81.9200000000	1.40386361975	20.6281638728	4.54812384872	93.3846927096
82.4200000000	1.40809098383	20.6896567174	4.54858843131	94.3800072907
82.9200000000	1.41233130225	20.8095968644	4.56175370493	92.6482879085
83.4200000000	1.41658445869	20.4347912828	4.52048573537	94.7461392605
83.9200000000	1.42085033786	20.2716007082	4.50239943898	94.8923719754

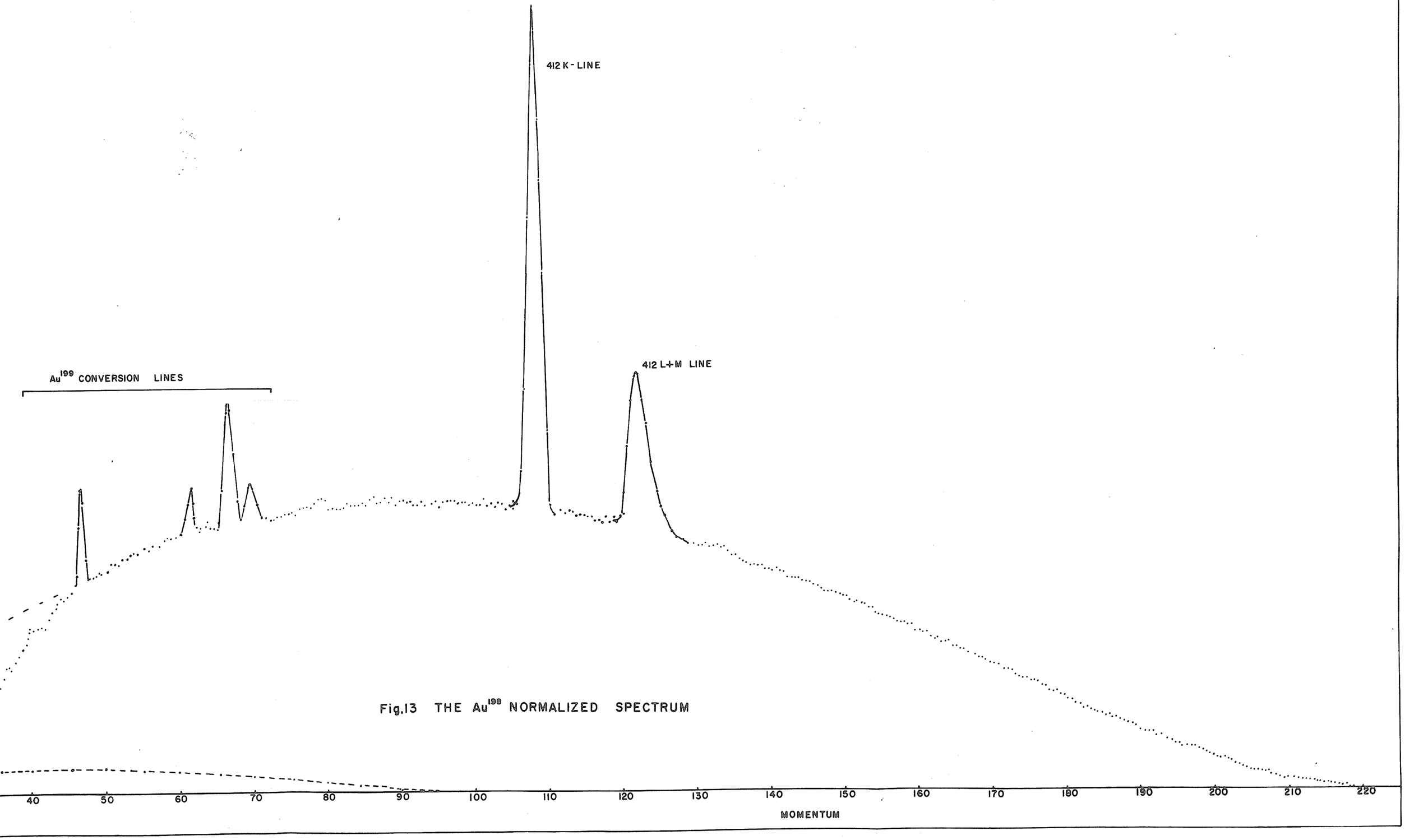

Fig.13 THE Au^{198} NORMALIZED SPECTRUM

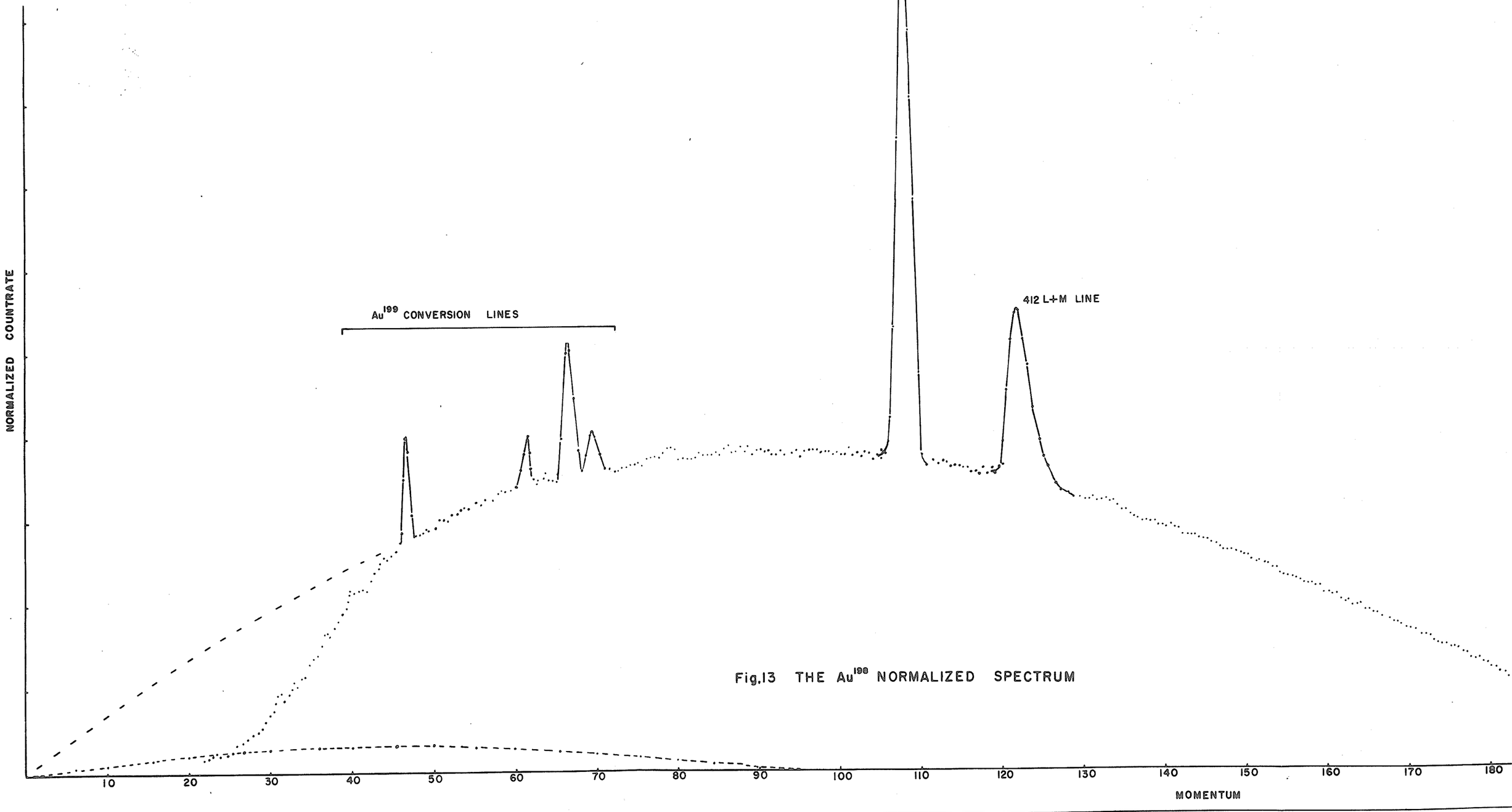

Fig.13 THE Au^{198} NORMALIZED SPECTRUM

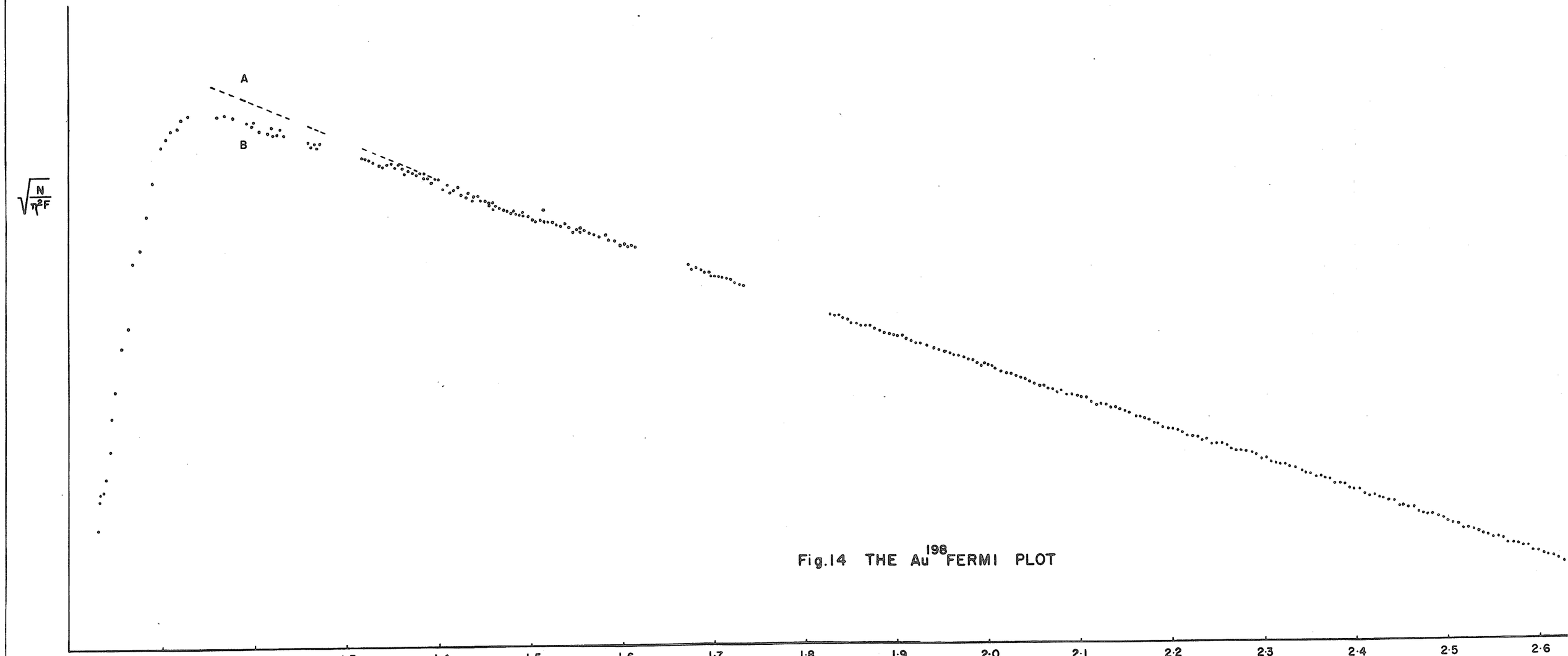

Fig.14 THE Au^{198} FERMI PLOT

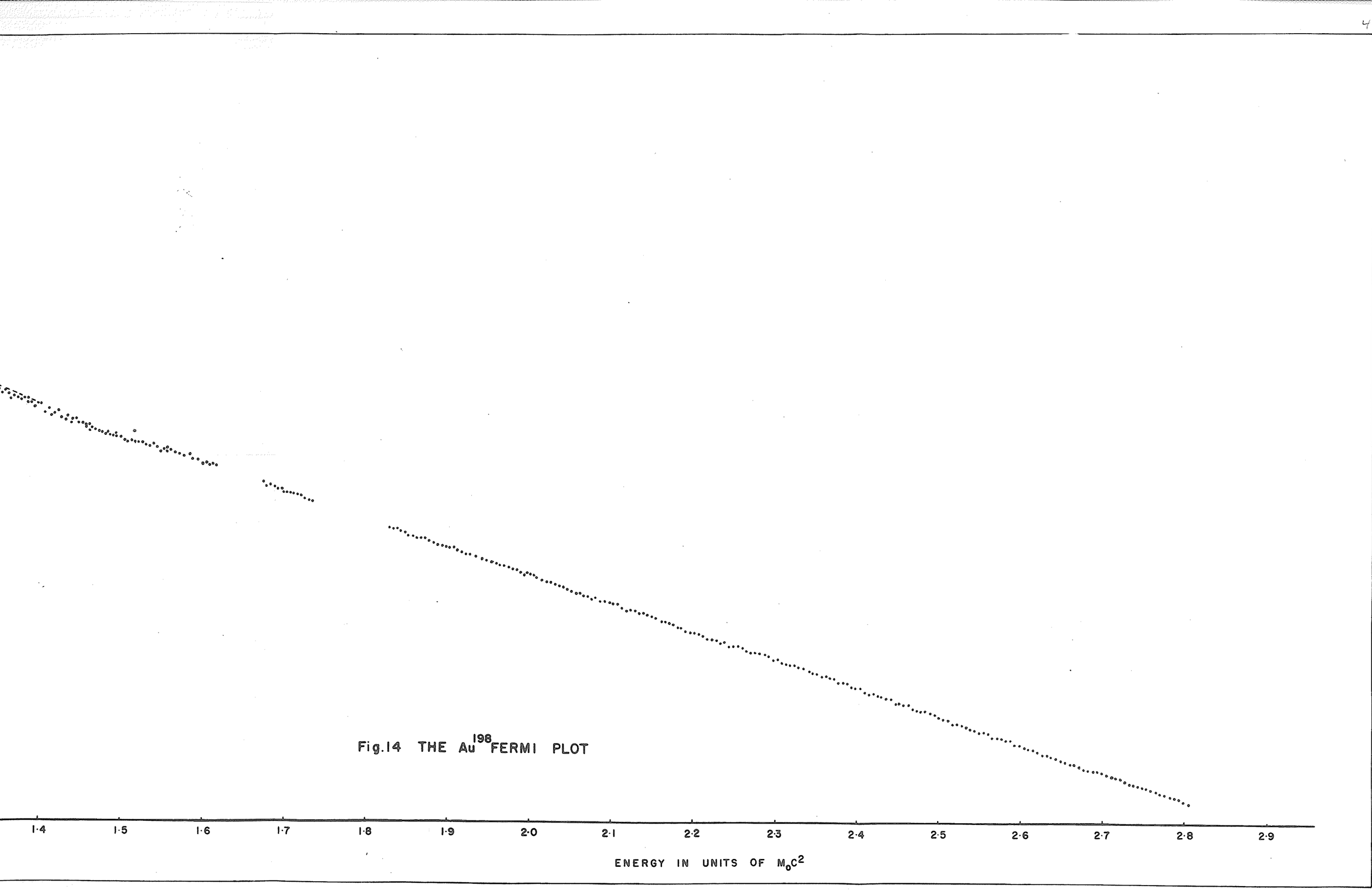

Fig.14 THE Au^{198} FERMI PLOT

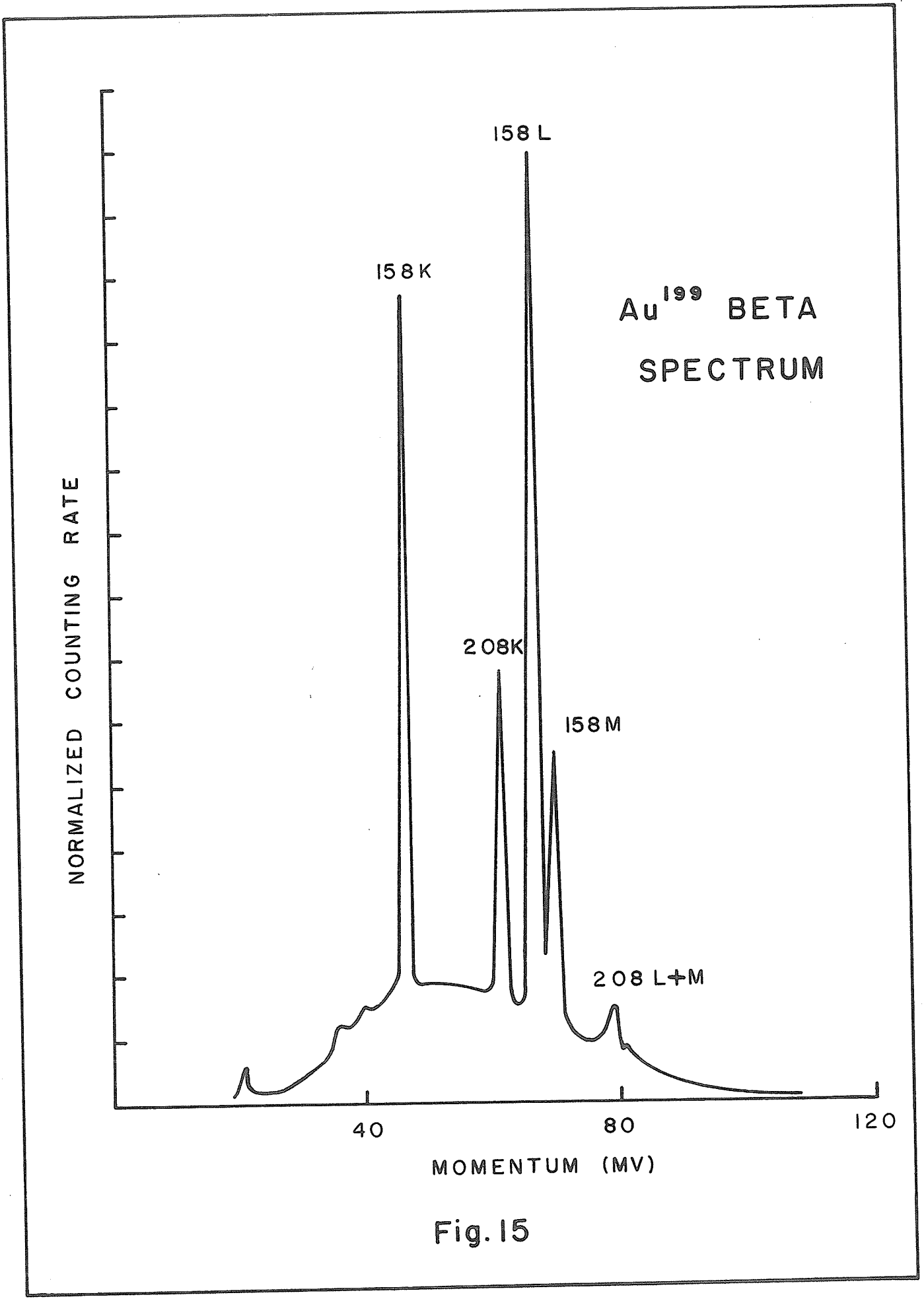
158 L
158 K
Au 199 BETA
SPECTRUM
208K
158 M
208 L+M
NORMALIZED COUNTING RATE
40
80
120
MOMENTUM (MV)

Fig. 15

momentum spectrum must be reconstructed for the 0 - 55 mv. region where the detector efficiency is less than 100%. From the Fermi plot for the Au^{199}, three line segments occur indicating the presence of three beta groups. In order to determine the relative intensities of these groups, the method of separating the composite Fermi plot into its component parts discussed in section (I - 1) was employed.

Reconstructing the feeds, assuming an allowed shape for each, and summing the three component spectra gave a total continuum area of 2.7845 in arbitrary units. The relative beta transition intensities for the three components were 6%, 71.4%, and 22.6% for the 460 kev., the 296 kev., and the 250 kev. β-groups respectively. The conversion line areas for the 158 L and M lines, and the 208 K line, are 0.515, 0.177, and 0.169, in the same units. Since the areas of the Au^{199} lines superposed on the Au^{198} spectrum were known, the total continuum area present could be calculated. This method was employed in calculating the percentage Au^{199} in two Au^{198} runs. Values of 2.1% and 2.2% Au^{199} contaminant were obtained.

The $\log_{10}$ ft values were determined for the partial β-feeds in both isotopes. The values obtained were:

Au^{198}:	Energy	$\log_{10}$ ft
	282 kev.	7.5
	960 kev.	7.3
	1370 kev.	11.4

Au^{199}:	Energy	$\log_{10}$ ft
	249 kev.	6.2
	296 kev.	5.8
	461 kev.	7.6

(3) Gamma Ray Investigations in Au^{198}:

In the conversion coefficient calculations, the relative gamma ray intensities for the Hg^{198} isotope must be known. The intensity ratios were found by shape analysis.

The gamma ray spectrum associated with the decay of Au^{198} is pictured in Fig. 16. The intensity of the high energy gamma ray is approximately 0.25% so a precise determination of the spectrum is essential.

A circuit for removing pulses produced by two coincident gamma rays entering the detector simultaneously was built[19]. If these pulses are not removed, they produce too many higher energy counts. In the case of a spectrum with a weak high energy gamma ray component like that found in Au^{198}, the intensity of the high energy gamma ray may be artificially increased.

Fig. 17 represents the block diagram of the circuit. The detectors are integral line scintillation detectors available commercially from Harshaw Manufacturing Co. Ltd.+ The linear amplifiers are manufactured by Nuclear Enterprises++ and have model number NE5202

+ Harshaw Manufacturing Co. Ltd., Cleveland, Ohio.

++Nuclear Enterprises, 550 Berry St., Winnipeg, Man.

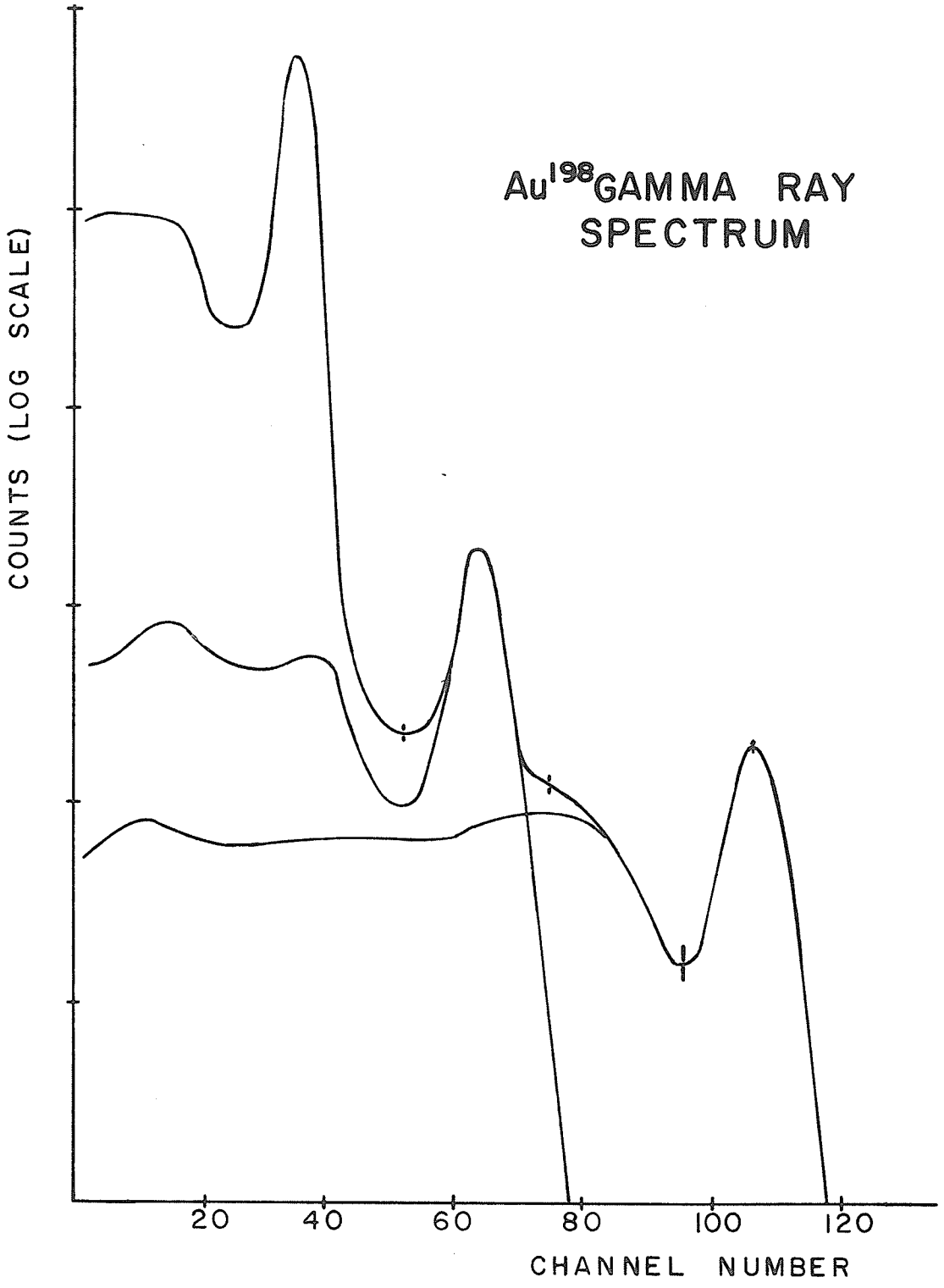
Au198 GAMMA RAY SPECTRUM
COUNTS (LOG SCALE)
20
40
60
80
100
120
CHANNEL NUMBER

Fig.16

BLOCK DIAGRAM OF CIRCUIT FOR REMOVING SUM PULSES

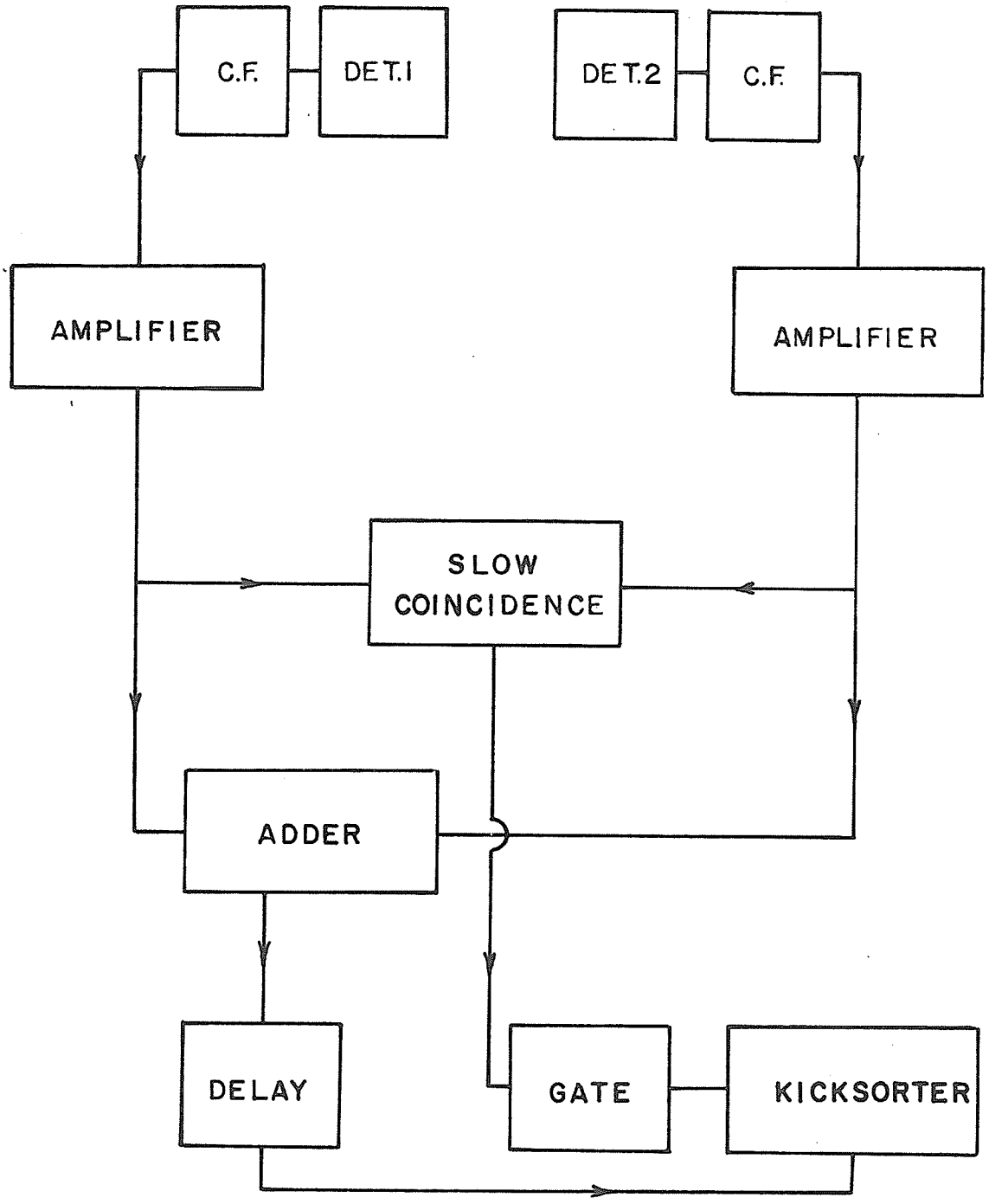

Fig. 17

The kicksorter is a product of Computing Devices of Canada Ltd.+, model AEP2230C while the slow coincidence unit was built in the Department.

Consider the illustrations below.

(a)

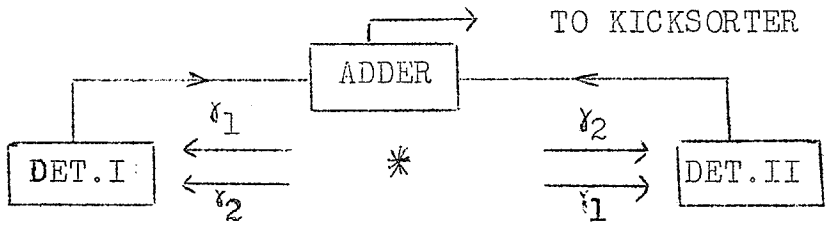

(b)

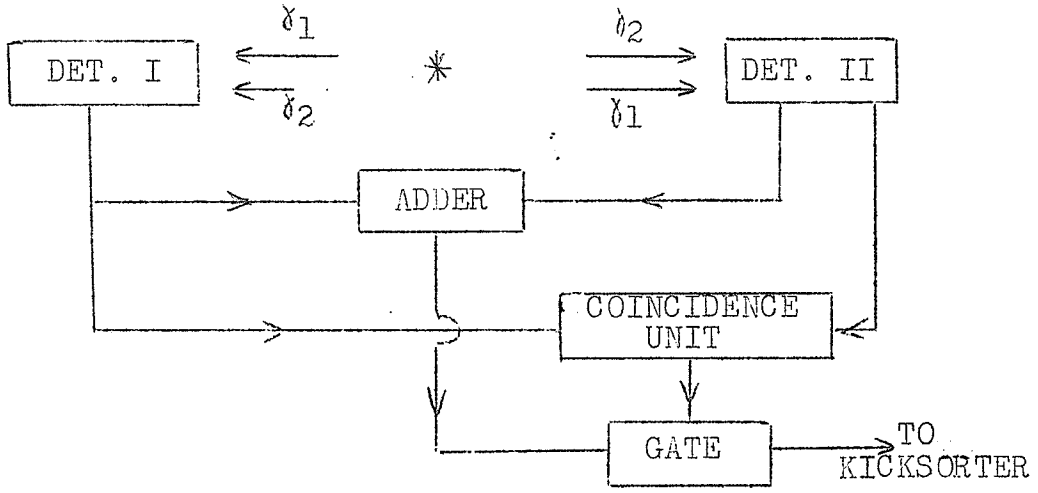

In case (a), signals reaching the kicksorter are due to the following possible detection combinations; - $(\gamma_1 + \gamma_2)_I$; $(\gamma_{1I} + \gamma_{2II})$; $(\gamma_{2I} + \gamma_{1II})$; $(\gamma_1 + \gamma_2)_{II}$, and single γ events.

In case (b), where the coincident event is employed, contributions to the output signals are due to $(\gamma_{1I} + \gamma_{2II})$ and $(\gamma_{2I} + \gamma_{1II})$.

+ Computing Devices of Canada Ltd., Ottawa, Ontario.

If both detectors are identical models and equidistant from the gamma emitting source, the source solid angle subtended by each detector is the same. For two cascading γ-rays γ_1 and γ_2, the number of counts produced by both γ-rays entering Detector I simultaneously is proportional to $(e_{I1}\omega_{I1})(e_{I2}\omega_{I2})$. Here the e's represent efficiency of detection for energies 1 and 2 by Detector I. The ω's are the solid angles at Detector I for energies 1 and 2, and are clearly equal since the solid angle is simply a geometrical quantity. Thus the number of sum counts is $\propto (e_{I1}e_{I2})\omega_I^2$.

In Detector II, the same argument gives the number of pulses produced by γ_1 and γ_2 entering the detector simultaneously as $\propto (e_{II1}\omega_{II1})(e_{II2}\omega_{II2})$ or $\propto (e_{II1}e_{II2})\omega_{II}^2$. But if the detectors are identical, the efficiency of detecting energy 1 or 2 is the same in both. Thus $e_{I1} = e_{II1} = e_1$, and

$e_{I2} = e_{II2} = e_2$, so that the total number of pulses produced by γ_1 and γ_2 entering Detector I or II simultaneously is $\propto 2e_1e_2\omega^2$, the geometry being the same for both.

For both detectors feeding the kicksorter as shown, an output from Detector I can sum with an output from Detector II, thus producing a sum pulse again. For γ_1 entering Detector I, and γ_2 entering Detector II, the number of sum pulses produced by cascading γ_1 and γ_2, will be proportional to $(e_{I1}\omega_{I1})(e_{II2}\omega_{II2})$. For γ_1 entering Detector II and γ_2 entering Detector I, the number of sum pulses is proportional to $(e_{I2}\omega_{I2})(e_{II1}\omega_{II1})$. But $e_{I2} = e_{II2} = e_2$, $e_{I1} = e_{II1} = e_1$, and $\omega_{I1} = \omega_{I2} = \omega_{II1} = \omega_{II2} = \omega$ so that the combined contribution is again $\propto 2e_1e_2\omega^2$. The total sum contributions from both summing methods is $\propto 4e_1e_2\omega^2$.

In determining the shape of the gamma ray spectrum, the two signal outputs are set to the same energy level by examining a mono-energetic gamma ray source through each detector system separately. The amplifier for each detector is set to locate the photo-peak of this mono-energetic γ-source in the same channel in the kicksorter. Once this has been

done, the two outputs are fed into the kicksorter through the adder circuit.

To remove the sum pulses, the kicksorter must be set to the coincidence mode. This mode requires a gating pulse before the input circuit to the kicksorter can pass a signal. The output from the slow coincidence unit can be used as a gating pulse so that signals register in the kicksorter only when pulses from Detectors I and II are in coincidence. The resolving time of the slow coincidence unit used was 1 microsecond. Thus if γ_1 entered Detector I and γ_2 entered Detector II, or vice versa, within 1 microsecond of each other, the sum pulse produced in the adder circuit was registered in the kicksorter. The coincidence spectrum was run twice as long as the singles spectrum in order to remove contributions due to γ_1 and γ_2 entering only one detector. These could not produce a gating pulse from the coincidence unit.

The spectra which were analyzed had the sum pulses removed in this way. However, the contribution to the total spectrum for the high energy gamma ray

was found to be of the order of 1%, so as it turns out the circuit was not necessary for this particular investigation, but this result could not be arrived at in advance. The background counting rate was determined by performing a run without a source.

(4) Gamma Ray Shape Analysis:

Once the gamma ray spectrum was obtained with sum pulses and background pulses removed, the relative component gamma ray intensities could be determined. The Au^{198} spectrum as shown in Fig. 16 contained three major gamma ray energies. Each gamma ray component had its own photo-peak and associated Compton distribution. In dissecting the spectrum into its component parts, the highest energy gamma ray and its Compton distribution were removed first. In doing this, a mono-energetic γ-ray, with approximately the same photo-peak energy as the component being subtracted, was run separately in order to determine the true photo-peak to Compton relationship. Plotting the spectra on a log scale allowed the calibration peak to be fitted under the photo-peak and hence the whole component contribution could be subtracted. The 1278 kev. γ-ray in Na^{22} was used as a calibration

source to "unpeel" the 1088 kev. γ-ray. Cs^{137} with a single γ-ray of energy 662 kev., was used as a calibration in unpeeling the 676 kev. γ-ray. The 412 kev. γ-ray distribution then remained alone. The photo-peaks for the three energies were then plotted on linear paper and their relative areas were determined. Tabulated values of crystal efficiency as a function of source distance, crystal size, and γ-ray energy[20], were then consulted to determine the relative efficiencies for the three different energy peaks. Then from a curve[21] which gives the "photo-peak to total intensity ratio" for different energy γ-rays, the γ-ray transition intensities could be deduced. Thus

$$N_{\gamma\ \mathrm{TOTAL}} = \frac{\text{Peak area}}{\text{Efficiency x Peak area to total intensity}}$$

Using this relation, the γ-ray intensities relative to the 412 kev. transition were calculated. The results for two runs are shown in Table 2 below.

TABLE 2

	412 kev.	676 kev.	1088 kev.
	1	.0097	.0025
	1	.0106	.0032
Av.	1	.0101	.0028

(5) Theoretical α_K Considerations:

In order to determine the intensity of the low energy Au^{198} beta feed, the Au^{198} gamma ray spectrum as well as the beta spectrum must be utilized. From the γ-ray spectrum, the relative intensities of the three γ-rays with energies 412 kev., 676 kev., and 1088 kev. were obtained.

A method for determining simultaneously the low energy β-feed intensity and the K-conversion coefficient for the 412 kev. transition was deduced as follows. Let the intensity of the low energy β-feed be x and the 960 kev. β-feed be (1 - x). (The 1370 kev. β-feed is known to be less than 0.03%[22] so was ignored in the calculations.) If a_K, a_L, and a_M are the K, L, and M conversion line areas for the 412 kev. transition, then, since the conversion lines for the 676 kev. and 1088 kev. are negligibly small, reference to Fig. 12(a) will show that

No. of 412 conversion electrons (N_{ce412}) per disintegration + No. of 412 γ-ray photons per disintegration + No. of 1088 γ-ray photons per disintegration = 1 . . . (V - 1)

Or, in another form,

$$\frac{(a_K + a_L + a_M)_{412}}{\text{disintegration}} + \frac{\text{No. of 412 kev. } \gamma\text{'s}}{\text{disintegration}} +$$

$$\frac{\text{No. of 1088 kev. } \gamma\text{'s}}{\text{disintegration}} = 1 \qquad \ldots (V - 2)$$

$$\text{If } \quad p = \frac{\text{No. of 1088 kev. } \gamma\text{'s}}{\text{No. of 412 kev. } \gamma\text{'s}} \qquad \ldots (V - 3)$$

then

$$\frac{\text{No. of 412 kev. } \gamma\text{'s}}{\text{disintegration}}(1 + p) = 1 - \frac{(a_K + a_L + a_M)_{412}}{\text{disintegration}}$$

and finally

$$\frac{\text{No. of 412 kev. } \gamma\text{'s}}{\text{disintegration}} = \frac{1 - \frac{(a_K + a_L + a_M)_{412}}{\text{disintegration}}}{1 + p} \qquad \ldots (V - 4)$$

Also from Fig. 12(a)

$$\frac{x}{1 - x} = \frac{\frac{\text{No. of 1088 kev. } \gamma\text{'s}}{\text{disintegration}} \text{ No. of 676 kev. } \gamma\text{'s}}{\text{No. of 412 kev. } \gamma\text{'s} + \frac{(a_K + a_L + a_M)_{412}}{\text{disintegration}} - \text{No. of 676 kev } \gamma\text{'s}} \qquad \ldots (V - 5)$$

But the K-conversion coefficient for the 412 kev. transition is

$$\alpha_K = \frac{\frac{a_K}{\text{disintegration}}}{\frac{\text{No. of 412 kev. } \gamma\text{'s}}{\text{disintegration}}} = \frac{\frac{a_K (1 + p)}{\text{disintegration}}}{1 - \frac{(a_K + a_L + a_M)_{412}}{\text{disintegration}}} \qquad \ldots (V - 6)$$

If A is the total area of the Au^{198} beta spectrum, then A represents the total number of disintegrations. Thus,

$$\alpha_K = \frac{\frac{a_K(1+p)}{A}}{1 - \frac{(a_K + a_L + a_M)_{412}}{A}} = \frac{a_K(1+p)}{A - (a_K + a_L + a_M)_{412}} \quad . \quad . \quad . \quad (V - 7)$$

The area A_1 of the 960 kev. beta feed can be given in terms of the total continuum, namely

$$A = \frac{A_1}{1 - x} \quad . \quad . \quad . \quad (V - 8)$$

So in terms of the 960 kev. beta transition

$$\alpha_K = \frac{a_K (1+p)}{\frac{A_1}{1-x} - (a_K + a_L + a_M)_{412}} \quad . \quad . \quad . \quad (V - 9)$$

Also $$\frac{x}{1-x} = \frac{\text{No. of 676 } \gamma\text{'s} + \text{No. of 1088 } \gamma\text{'s}}{\text{No. of 412 transitions} - \text{No. of 676 } \gamma\text{'s}}$$

$$= \frac{\text{No. of 676 } \gamma\text{'s} + \text{No. of 1088 } \gamma\text{'s}}{\text{No. of 412 } \gamma\text{'s } N_{ce412} - \text{No. of 676 } \gamma\text{'s}} \quad . \quad . \quad . \quad (V - 10)$$

The conversion electrons $N_{ce412} = a_K + a_{L+M}$ can be represented by

$$N_{ce412} = N_{\gamma 412} \left(\alpha_K + \frac{a_{L+M}}{a_K} \alpha_K \right)$$

so (V - 10) takes the form

$$\frac{x}{1-x} = \frac{\text{No. of } 676\ \gamma\text{'s} + \text{No. of } 1088\ \gamma\text{'s}}{N_{\gamma 412}\ (1+\alpha_K + \frac{a_{L+M}}{a_K}\alpha_K) - \text{No. of } 676\ \gamma\text{'s}} \quad \ldots \text{(V - 11)}$$

From (V - 11) and (V - 9), α_K and x can be determined.

(6) Determination of the α_K Conversion Coefficient:

Once the relative gamma ray intensities were established, the only remaining quantity to be determined before (V - 9) and (V - 11) were solvable was A_1, the area of the 960 kev. beta feed.

The Fermi plot for the complete Au^{198} spectrum was found to be linear from the end point of 960 kev. down to approximately 300 kev. Below this value, the low energy Au^{198} feed starts to contribute to the Fermi plot. As a first approximation, without any prejudice to the final result, the 960 β -feed was assumed linear below 300 kev. so its continuum could be constructed. The area of the continuum found in this way was 11.6103 in arbitrary units for Run #1 and 14.464 for Run #2. Using these values for A_1, along with the relative γ-ray intensities $1_{412}:0.0101_{676}:0.0028_{1088}$

and conversion line areas $a_K = 0.332$, $a_{L+M} = 0.162$, for Run #1, and $a_K = 0.422$, $a_{L+M} = 0.200$ for Run #2, α_K and x were computed.

For Run #1, $\alpha_K = 0.02965$ and $x = 0.0124$: for Run #2, $\alpha_K = 0.03017$ and $x = 0.0124$. The average values are $\alpha_K = 0.0299$ and $x = 0.0124$. This determination of α_K is in exact agreement with theoretical values of Rose, and Sliv and Band. The uncertainty in α_K was estimated to be 2% so that the final value is $\alpha_K = 299 \pm 6 \times 10^{-4}$. Table 3 compares the value of α_K to those of other workers.

TABLE 3

	Value	Author
I.E.C.# Method	280 ± 15	De Vries[16]
	280 ± 15	Hultberg et al[23]
	280 ± 15	Frey et al[24]
	303 ± 5	Bergkvist and Hultberg[25]
Other Methods	305 ± 10	Pettersson et al[26]
	301 ± 4.5	Lewin et al[27]
P.B.S. Method	300 ± 10	Hubert[28]
	281 ± 5	Wapstra et al[15]
	285 ± 15	Newbolt et al[29]
	282 ± 10	Hamilton et al[17]
	302 ± 6	Present work
	295 ± 6	
Theory	302	Rose[5]
	298	Sliv and Band[6]

Internal-External Conversion.

The value of α_{L+M} can be determined from the relationship

$$\frac{\alpha_K}{\alpha_{L+M}} = \frac{\frac{a_K}{\text{No. of corresponding } \gamma\text{'s}}}{\frac{a_{L+M}}{\text{No. of corresponding } \gamma\text{'s}}} = \frac{a_K}{a_{L+M}}$$

Using this method, $\alpha_{L+M} = 146 \pm 10 \times 10^{-4}$ for Run #1, and $\alpha_{L+M} = 144 \pm 3 \times 10^{-4}$ for Run #2. The average value, $\alpha_{L+M} = 145 \pm 3 \times 10^{-4}$ agrees, within experimental error, with the theoretical value 146×10^{-4} determined by Rose(5).

The average value of x calculated was x=0.0124. From equation (V - 11) x can be computed as a function of α_K. For $\alpha_K = 0$, substituting known values of a_K, a_{L+M}, and the γ-ray intensities, gives $x = 0.0130$. For $\alpha_K = 0.03$, the theoretical value, $x = 0.0124$. Thus x is not critically dependent on the α_K used. Subtracting $x = 1.24\%$ from the total Au^{198} feed leaves the resulting Fermi plot straight down to 100 kev. This indicates the transition is allowed and also justifies the assumption that the Fermi plot could be assumed straight in the α_K determination. The contribution is small enough that a determination of α_K assuming $x = 0$ gives a value $\alpha_K = 0.0296$, i.e. a 1% change. This still agrees with theory to within experimental error.

Chapter VI

THE SHAPE FACTOR FOR THE 960 KEV. β -FEED

Introduction:

Although the Fermi plot of the 960 kev. β - feed looked straight after the 1.24% low energy component was subtracted (see Fig. 14-B), in order to compare the result with that obtained by other workers, it was decided that the observations would be fitted to the two major shape factor forms used in the analysis of Au^{198} so far. These shape factors are given by:

$$C(\omega) = k(1 + a\omega + b\omega^2 + C/\omega) \quad . \quad . \quad .(VI - 1)$$

$$C(\omega) = k(1 + g(\omega_o - \omega))^2 \quad . \quad . \quad .(VI - 2)$$

Equation (VI - 1) was introduced by Kotani[30] while equation (VI - 2) was derived by Wapstra[31]. The theory, which is lengthy and involved, will not be discussed here.

The points in the Fermi plot were converted to the $C(\omega)$ vs.ω form using equation (I - 14). ie.

$$\frac{N}{S\eta^2 f(\omega - \omega_o)^2} = KC(\omega) \quad . \quad . \quad .(VI - 3)$$

A plot of $C(\omega)$ vs.ω for one of the runs is shown in Fig. 18(A). The "allowed" shape function L_o is not presupposed.

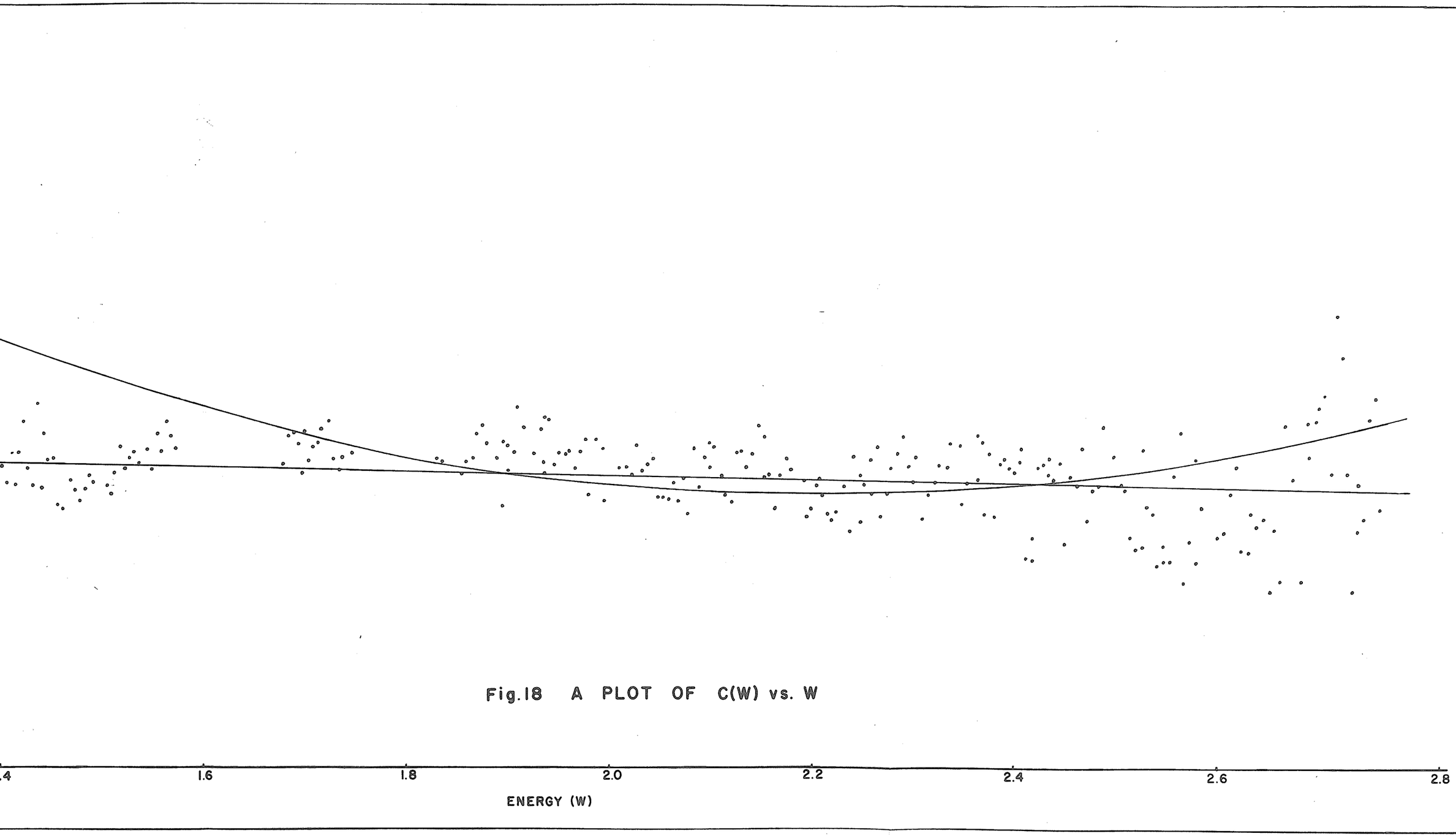

Fig.18 A PLOT OF C(W) vs. W

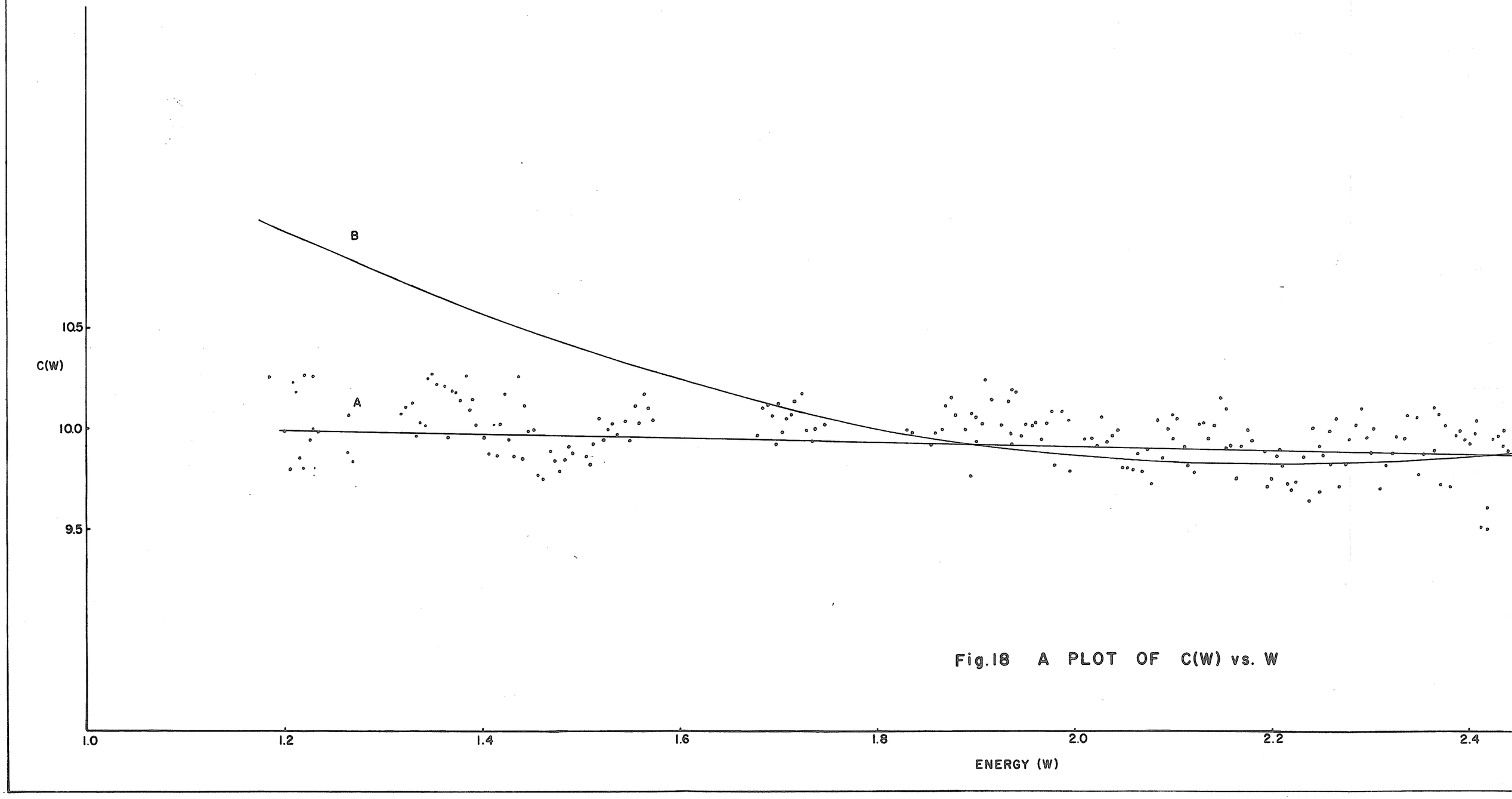

Fig.18 A PLOT OF C(W) vs. W

(1) Least Squares Procedure:

In determining the curves of best fit through the $C(\omega)$ vs. ω distribution for forms (VI - 1) and (VI - 2), the method of least squares was used. A short description of this procedure is now given.

By definition, $\delta = (C(\omega) - k(1 + a\omega + b\omega^2 C/\omega))^2$ is the square of the distance between one experimentally determined point $C(\omega)$, and the corresponding curve, fitting the point distribution at that energy value ω. For n points the total δ is given by

$$\delta_T = \sum_{i=1}^{n} (C(\omega) - k(1 + a\omega + b\omega^2 + C/\omega))^2 \qquad (VI - 4)$$

or, in another form where k is multiplied inside the bracket.

$$\delta_T = \sum_{i=1}^{n} (C(\omega) - (k + a_1\omega + a_2\omega^2 + a_3/\omega))^2 \qquad (VI - 5)$$

In order that the curve fit is the best fit, corresponding to a minimum δ_T, δ_T is differentiated with respect to k, a_1, a_2, and a_3, and the equations so obtained are set equal to zero. Thus;

$$\frac{\partial \delta}{\partial k} = \Sigma(C(\omega) - (k + a_1\omega + a_2\omega^2 + a_3/\omega)) = 0 \qquad (VI - 6)$$

$$\frac{\partial \delta}{\partial a_1} = \Sigma\left(C(\omega) - (k + a_1\omega + a_2\omega^2 + a_3/\omega)\right)\omega = 0 \qquad \text{(VI - 7)}$$

$$\frac{\partial \delta}{\partial a_2} = \Sigma\left(C(\omega) - (k + a_1\omega + a_2\omega^2 + a_3/\omega)\right)\omega^2 = 0 \qquad \text{(VI - 8)}$$

$$\frac{\partial \delta}{\partial a_3} = \Sigma\left(C(\omega) - (k + a_1\omega + a_2\omega^2 + a_3/\omega)\right)\frac{1}{\omega} = 0 \qquad \text{(VI - 9)}$$

If $C(\omega)$ is replaced by y, and $\sum_{1=1}^{n}$ is abbreviated by Σ, the equations can be re-written in the form

$$\Sigma y = nk + a_1\Sigma\omega + a_2\Sigma\omega^2 + a_3\Sigma\frac{1}{\omega} \qquad \text{(VI -10)}$$

$$\Sigma y\omega = k\Sigma\omega + a_1\Sigma\omega^2 + a_2\Sigma\omega^3 + a_3 n \qquad \text{(VI -11)}$$

$$\Sigma y\omega^2 = k\Sigma\omega^2 + a_2\Sigma\omega^3 + a_2\Sigma\omega^4 + a_3\Sigma\omega \qquad \text{(VI -12)}$$

$$\Sigma\frac{y}{\omega} = k\Sigma\frac{1}{\omega} + a_1 n + a_2\Sigma\omega + a_3\Sigma\frac{1}{\omega^2} \qquad \text{(VI -13)}$$

This can be represented in matrix notation by

$$\begin{pmatrix} n & \Sigma\omega & \Sigma\omega^2 & \Sigma\frac{1}{\omega} \\ \Sigma\omega & \Sigma\omega^2 & \Sigma\omega^3 & n \\ \Sigma\omega^2 & \Sigma\omega^3 & \Sigma\omega^4 & \Sigma\omega \\ \Sigma\frac{1}{\omega} & n & \Sigma\omega & \Sigma\frac{1}{\omega} \end{pmatrix} \begin{pmatrix} k \\ a_1 \\ a_2 \\ a_3 \end{pmatrix} = \begin{pmatrix} \Sigma y \\ \Sigma y\omega \\ \Sigma y\omega^2 \\ \Sigma\frac{y}{\omega} \end{pmatrix} \qquad \text{(VI-14)}$$

After the 4 x 4 matrix on the left hand side of the equation has been diagonalized, (the right hand side of the equation undergoing the same operation for each step in the diagonalization process on the left), the values k, a_1, a_2, and a_3 can be equated to the corresponding element in the same row on the right hand side. Thus the coefficients corresponding to the curve of best fit are then known.

In performing a least squares procedure on equation (VI - 2), the approach is identical, only here there are two coefficients to be determined and thus a 2 x 2 matrix must be diagonalized.

(2) Statistical Weighting of the Points:

The statistical accuracy of the experimentally obtained points varies, so that in determining the curve of best fit through the $C(\omega)$ vs. ω distribution, those points known to greater precision should be weighted accordingly.

In the original determination of the momentum distribution, the counting rate at increasing millivolt settings was recorded. The statistical uncertainty in the counting rate (C.R.) is given by $\sqrt{C.R.}$, and is

referred to as the Standard Deviation from C.R. In "Statistical Adjustment of Data" by Deming, weight is given as $\omega \propto \frac{1}{\sigma_f^2}$, where σ_f is the "standard deviation" of the function, and in this case is $\sqrt{C.R.}$.

For the form $C(\omega)$ however, since $N = \frac{C.R.}{mv.}$, the dependence on C.R. is given by

$$C(\omega) = \frac{C.R.}{S\eta^2(mv.)f(\omega - \omega_o)^2}$$

The uncertainty in $C(\omega)$ due to the uncertainty in the C.R. is

$$\sigma_f = \frac{\sqrt{C.R.}}{\eta^2(mv.)f(\omega - \omega_o)^2}$$

Therefore, the weighting factor for the i^{th} point is given by

$$\omega_i = \frac{S^2\eta^4(mv.)^2f^2(\omega - \omega_o)^4}{C.R.} \qquad \text{(VI -15)}$$

(3) Determination of the Shape Factor Coefficients:

Using the weighting factor described above, the I.B.M. Computer at the University of Manitoba was programmed to perform the least squares fit of the shape factor to the experimentally determined $C(\omega)$ vs. ω distribution. The results for the coefficients are tabulated in Table 4.

TABLE 4

TABLE OF SHAPE FACTOR COEFFICIENTS (L_o excluded)

(a) $c(\omega) = k(1 + a\omega + b\omega^2 + c/\omega)$

RUN 1.

ω_o	k	a	b	c
2.879	11.8157	-0.0606	0.0048	-0.1040
2.880+	10.7232	-0.0043	-0.0082	-0.0606
2.881	9.6022	0.0667	-0.0061	-0.0062
2.882	8.9383	0.1206	-0.0361	0.2960

$\Delta\omega_o = \pm 0.0014$ = the uncertainty in the end point.

RUN 2.

2.878	13.7863	-0.2187	0.0347	-0.2417
2.879+	11.3769	-0.1448	0.0194	-0.1715
2.880	10.6838	-0.1129	0.0117	-0.1498
2.881	9.6031	-0.0578	-0.0007	-0.1061

$\Delta\omega_o = \pm 0.0015$

Hamilton et al[17]	0.33	0.075	0

(b) $c(\omega) = k(1 + g(\omega_o - \omega))^2$

RUN 1.

ω_o	k	g
2.879	9.9174	0.00456
2.880+	9.8735	0.00562
2.881	9.8297	0.00669
2.882	9.7866	0.00774

RUN 2.

2.878	7.8862	0.0111
2.879+	7.8561	0.0122
2.880	7.7857	0.0134
2.881	7.7512	0.0144

Chabre et al[14]	k	0.034 ± 0.004
Wapstra [15]	k	0.065 ± 0.01
De Vries [16]	k	0.083 ± 0.01

+ End point determined from the Fermi Analysis.
(i) $\omega_o = 2.880 \pm 0.0014 = 960.7 \pm 0.7$ kev.
(ii) $\omega_o = 2.879 \pm 0.0015 = 960.2 \pm 0.8$ kev.

For the shape factor proposed by Kotani, the values of the coefficients obtained vary considerably with the choice of the end-point ω_o. For different ω_o values, all within the error limits on the experimental end point, the coefficients can either be made small or quite large depending on the choice of ω_o. The conclusion drawn was that the presence of the term in $\frac{1}{\omega}$ allows a sensitive curve fit to be made to the points, but permits very little reliance to be given the coefficients thus determined. However, the coefficients listed are small in general, and in the case of the coefficient of ω, found to be significantly lower than that proposed by Hamilton et al[17] whose coefficients were used in determining curve (B) in Fig. 18.

For the shape factor proposed by Wapstra, the values of g determined for the two runs differ in magnitude. The values of g are so small, however, that slight differences in source quality are significant enough to produce the difference. There is a slight variation in g with the choice of ω_o, but the values in general are at least three times smaller than any other reported values.

The coefficients in the shape factor determination were also obtained with unit weighting of the points. The values were essentially the same so that

the same conclusion could be drawn from either weighted or non-weighted values.

The coefficients for a shape factor of the form $C(\omega) = a_o + a_1\omega + a_2\omega^2$, were also determined using the computer. The results were similar to those of form (VI - 1) as would be expected since the two equations are identical except for the missing $\frac{1}{\omega}$ term in the latter equation.

The shape factor coefficients were also determined when the point distribution was corrected for the allowed shape factor L_o. This was done in order to get an estimate of the deviation from the allowed shape for the Au^{198} Fermi plot. The L_o values vary from 0.88 to 0.83 and this is the form of the shape factor of Fig. 18 (A).

The coefficients determined for the case where L_o is included as a correction, are listed in Table 5. In the shape factor form proposed by Wapstra, g is now effectively zero, and the coefficients for the form proposed by Kotani are reduced. This is further evidence that the spectrum is allowed. Here the shape factor coefficients have no theoretical significance.

TABLE 5

TABLE OF SHAPE FACTOR COEFFICIENTS (L_o included)

(a) $c(\omega) = k(1 + a\omega + b\omega^2 + c/\omega)$

RUN 1.

ω_o	k	a	b	c
2.879	13.30	0.054	-0.016	-0.139
2.880	12.69	-0.017	-0.001	-0.095
2.881	10.10	0.130	-0.039	0.021
2.882	9.75	0.170	-0.039	0.039

$\Delta\omega_o = \pm 0.0014$

RUN 2.

2.879	12.010	-0.107	0.015	-0.150
2.880	9.022	0.057	-0.020	-0.022
2.881	8.735	0.079	-0.024	-0.004
2.882	8.295	0.115	-0.032	0.024

$\Delta\omega_o = \pm 0.0015$

(b) $c(\omega) = k(1 + g(\omega_o - \omega))^2$

RUN 1.

ω_o	k	g
2.878	11.845	-0.0024
2.879	11.754	-0.0020
2.880	11.699	-0.0017
2.881	11.606	-0.0011

RUN 2.

2.878	9.322	-0.00029
2.879	9.277	0.00009
2.880	9.233	0.00049
2.881	9.145	0.00127

(4) Conclusions:

The final conclusion made with regard to the Au^{198} 960 kev. β-feed, is that the shape is allowed within experimental error. Also, the 412 kev. conversion coefficients are in exact agreement with theoretical predictions. If a slight shape factor for the 960 kev. β-feed is included, the change in the 960 kev. β-continuum area is less than 1%. This in turn would change the α_K conversion coefficient by approximately 1% because of its dependence on the β-continuum. The resulting value of α_K would still agree with theory within experimental error.

Several other investigators have measured α_K for the 412 transition in Hg^{198} using methods other than the P.B.S. technique. Some have found that their values agreed with theory (See Table 3, p. 56). Thus it would seem reasonable to assume that source absorption and backing effects, coupled with possible instrumental distortion of the beta spectrum, could explain the shape factors proposed by other workers. Further, it would explain subsequent disagreement between computed α_K values and theoretical predictions, wherever the P.B.S. technique was employed.

APPENDIX

Properties of the Au^{199} Isotope

The Au^{199} decay scheme pictured in Fig. 12(b) has already been referred to but the main properties found during the present investigation will be outlined in this Appendix.

The Au^{199} beta continuum is shown in Fig. 15. The corresponding Fermi plot reveals three distinct line segments corresponding to the three beta groups. Separation of these feeds yielded end points of 461 $\pm$2 kev., 296 $\pm$2 kev., and 249 $\pm$3 kev. respectively, with corresponding relative intensities of 6.0 $\pm$0.3%, 71.4 $\pm$2%, and 22.6 $\pm$2%. Both the end points and intensities agree well with the results of other workers indicating the proper functioning of the spectrometer.

In order to determine the conversion coefficients for the de-excitation transitions in the daughter Hg^{199} nucleus, gamma ray work was performed in the same manner as for the Au^{198} isotope. The gamma ray spectrum for the Au^{199} isotope is illustrated in Fig. 19.

In determining the conversion coefficients the following method was used. From Fig. 12 (b) it

Fig. 19 Au^{199} GAMMA RAY SPECTRUM

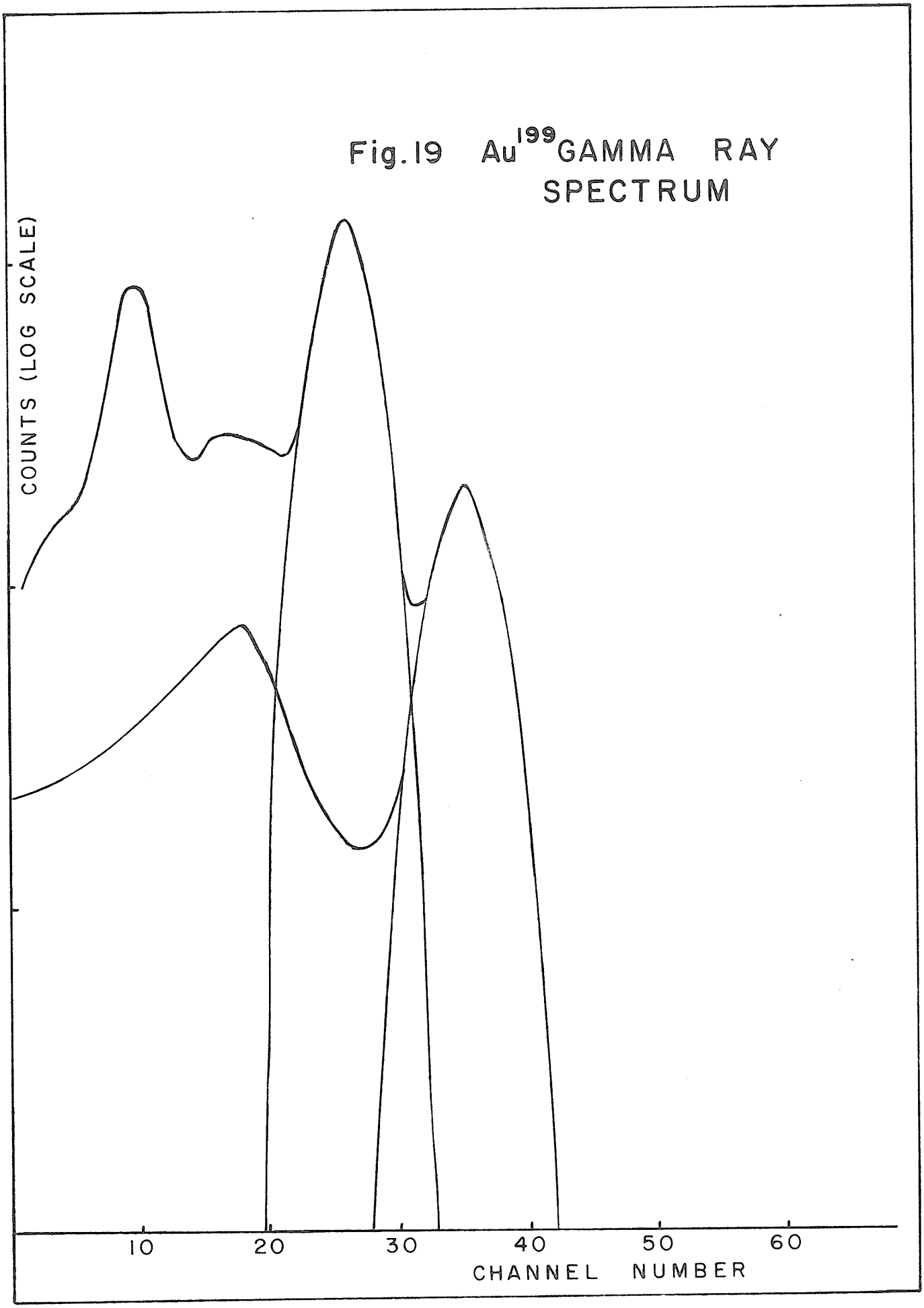

is apparent that

Intensity of 296 kev. β-group + Intensity of 250 kev. β-group = 0.94 of all transitions. . . I

This is so since 6% of the decay events are to the ground-state in Hg^{199} with no subsequent de-excitations. Another relation can be given by

(No.of 208 kev. transitions per disintegration) + (No.of 158 kev. transitions per disintegration) = 0.94, or,

$$\frac{\text{No.of 208 kev.transitions}}{\text{disintegration}} + \frac{\text{No.of 158 kev.transitions}}{\text{disintegration}} = 0.94 \quad \ldots \text{II}$$

i.e.

$$\frac{\text{No.of 208 kev. } \gamma\text{'s}}{\text{disintegration}} + \frac{\text{No.of 208 kev. conv.e's}}{\text{disintegration}} + \frac{\text{No.of 158 kev. } \gamma\text{'s}}{\text{disintegration}} + \frac{\text{No.of 158 kev. conv.e's}}{\text{disintegration}} = 0.94 \quad \ldots \text{III}$$

The beta continuum and conversion line areas were determined using a Beta Ray Spectrometer. The gamma ray intensities were determined using Scintillation apparatus, whose relative detection efficiency is different from that of the β-Spectrometer. Equating II and III and allowing for differences in the detector counting rates by introducing constants ε_1 and ε_2, gives

ε_2(no.of 208 γ's + No.of 158 γ's) + ε_1(No.of 158 conv. e's + No.of 208 conv. e's) = ε_1(No. of disintegrations in 300 kev. and 250 kev. β-groups)

Since ε_1 and ε_2 are relative, if we set $\varepsilon_1 = 1$, then

ε_2(No.of 158 γ's + No.of 208 γ's) = 0.94 (Total beta continuum area) - (No.of 158 and 208 conv. e's).

Using the values obtained in arbitrary units from an area measurement made on the beta spectrum.

ε_2(No.of 158 γ's + No.of 208 γ's) = 1.4245

From the gamma ray work, shape analysis gives the ratio of the 158 kev. gamma ray intensity to the 208 kev. gamma ray intensity as 4.55:1, and No.of 158 γ's + No.of 208 γ's = 80.416 in arbitrary gamma ray units. Thus ε_2 is found to be 0.018165.

In terms of the arbitrary beta continuum units

No.of 158 γ's = 1.16117 or 41.9 % in terms of the number of decay events.

Also,

No.of 208 γ's = 0.26324 or 9.2 % in terms of the number of decay events.

Since all the values are now in the same units, the conversion coefficients α_K, α_L, and α_M can thus be determined directly from the relations

$$\alpha_K = \frac{N_{ceK}}{N\gamma} , \quad \alpha_L = \cdot \quad \cdot \quad \cdot \quad \cdot \quad \cdot$$

The results are compared with those of other workers in Table 6.

TABLE 6

Transition Energy	K-Conversion Coefficient	Relative Conversion Electron Intensities*				Author
	α_K	K	L	M	NO	
158	-----	188	318	84	20	Cressman et al[32]
	0.33	200	298	104		de Shalit et al[33]
	$0.19^{+.15}_{-.06}$	147	245	83		Sherk et al[34]
	0.24	---	---	---		Siegbahn[35]
	$0.25 \pm .02$	172	305	103		Present work
208	---	100	20	5.9	1.2	Cressman et al
	0.78	100	18	7		de Shalit et al
	0.54^{+8}_{-19}	100	18	5		Sherk et al
	0.62	---	--	-	-	Siegbahn
	$0.66^{+}_{-}.04$	100	20	7		Present work

* The intensity of the 208 K-conversion line is arbitrarily set equal to 100.

The 158 kev. transition is from the 5/2- state to the 1/2- ground state. Thus the transition may be either E2 or M3. The theoretical α_K value is 0.29 for a 158 kev. E2 transition, and 26.5 for a 158 kev. M3 transition. The experimental value obtained was 0.25 ± 0.02, indicating the transition is pure E2. Although M1, E1, and M2 transitions would be forbidden here with the present spin and parity assignments, theoretical values of α_K were obtained for these transitions at an energy of 158 kev. The theoretical predictions are: M1, $\alpha_K = 1.87$, M2, $\alpha_K = 9.70$, and E1, $\alpha_K = 0.10$. Since the experimentally determined α_K does not agree at all with the first two, and the theoretical value for the E1 case still differs significantly from the experimental value, the assigned spins and parities can be assumed correct. Thus a pure E2 transition is predicted.

The 208 kev. transition is from the 3/2- state to the 1/2- ground state and can be either M1 or E2. The 208 kev. E2 transition has a theoretical α_K value of 0.152, while the 208 kev. M1 transition has a value of 0.836. The experimentally determined α_K was 0.66 ± 0.04. The percentage contributions made by the

E2 and M1 transitions can be obtained from the relation

$$0.66 = x(0.152) + (1 - x)(0.836).$$

Solving for x yields

$$x = 26.5\% \text{ E2}, \quad \text{and } x = 73.5\% \text{ M1}.$$

Hence the 208 kev. transition is 73.5% M1 and 26.5% E2.

The absolute intensities for the 208 kev. and 158 kev. transitions were also determined. The 158 kev. gamma ray represents 41.9% of the total number of decay events. The total number of 158 kev. conversion electrons in beta continuum units is 0.981 or 35.2%. So the 158 kev. transition represents 77.1% of all transitions. Similarly the 208 kev. transition represents 9.2% + 7.7% = 16.9% of all transitions. The remaining 6% are ground-state ground-state transitions. These values are in excellent agreement with the average values of 77%, 16%, and 6.4% respectively, given by the Nuclear Data Sheets.

REFERENCES

1) F. Reines, Annual Review of Nuclear Science, Vol. 10, 1960.

2) E. Fermi, Zeits. f. Physik 88, 161 (1934).

3) U.S. At. En. Commission, Publication ORNL-1459.

4) U.S. Nat. Bureau of Standards, Applied Math. Series, No. 13.

5) M.E. Rose, Internal Conversion Coefficients : North-Holland, Amsterdam, 1958.

6) L. A. Sliv and I. M. Band, Coefficients of Internal Conversion of Gamma Radiation, U.S.S.R. Academy of Sciences, Moscow, Leningrad, 1956.

7) O. V. Baeyer and O. Hahn, Physik Zeits., 11, 488 (1910)

8) F. Konopasek and R. D. Connor, Nucl. Instr. and Methods, 24, 66-73 (1963).

9) C. S. Wu and L. Feldman, Phys.Rev., 76, 697, 698 (1949).

10) Beta and Gamma Ray Spectroscopy, ed. K. Siegbahn, (North Holland) Appendix VII.

11) F. T. Porter, F. Wagner,Jr., and M. S. Freedman, Phys. Rev., 107, 135 (1957).

12) D. G. Douglas, Phys. Rev., 75, No. 12, 1960 (1949).

13) W. Van Wyngaarden and R. D. Connor, Can. J. Phys., March 1964 (in press).

14) M. Chabre and P. Depommier, J. Phys. Rad., 22 674 (1961).

15) A. H. Wapstra, G. J. Nijgh, Salomons-Grobben, and L. Th. M. Ornstein, Nucl.Phys., 9, 538 (1958).

16) C. De Vries et al, Nucl. Phys., 18, 454 (1960).

17) J. H. Hamilton, R. V. Stockendal, D. C. Camp, L. M. Langer, and D. R. Smith, Nucl. Phys., 36, 567 (1962).

18) B. D. Pate and L. Yaffe, Can. J. Chem., 33, 15 (1955).

19) S. O. Schriber, private communication, McMaster University, Hamilton, Ontario.

20) Naval Research Lab. Report No.4833, Oct. 5, 1956.

21) W. E. Mott and R. B. Sutton, Handbuch der Physik, Vol. 45, 127.

22) L. G. Elliot, M. A. Preston, and J. L. Wolfson, Can. J. Phys., 32, 153 (1953).

23) S. Hultberg, D. Horen, and J. M. Hollander, Nucl. Phys., 28, 471 (1961).

24) W. F. Frey, J. H. Hamilton, and S. Hultberg, Ark. Fys., 21, 383 (1962).

25) K. E. Bergkvist and S. Hultberg, Ark. Fys., (to be published).

26) B. G. Petterson, J. E. Thun, and T. R. Gerholm, Nucl. Phys., 24, 243 (1961).

27) W. H. G. Lewin, B. Van Nooijen, C. W. E. Van Eijk, and A. H. Wapstra, Nucl. Phys., 48, 159 (1951).

28) P. Hubert, Compt. Rend., 232, 2201 (1951).

29) B. Newbolt and J. H. Hamilton, quoted private communication in Ref. 17.

30) T. Kotani and M. Ross, Phys.Rev., 113, 622 (1959).

31) A. H. Wapstra, Nucl. Phys., 9, 519 (1958-1959).

32) P. J. Cressman and R.G.Wilkinson, Phys.Rev.,109, 872.

33) A. de-Shalit, O. Huber, and H. Schneider, Helv. Phys. Acta, 25, 279.

34) P. M. Sherk and R. D. Hill, Phys.Rev., 83, 1097 (1951).

35) K. Siegbahn, Arkiv. Fysik, 4, 223.